We are IntechOpen, the world's leading publisher of Open Access books Built by scientists, for scientists

4,800
Open access books available

122,000
International authors and editors

135M
Downloads

Our authors are among the

154
Countries delivered to

TOP 1%
most cited scientists

12.2%
Contributors from top 500 universities

CLARIVATE ANALYTICS BOOK CITATION INDEX INDEXED

WEB OF SCIENCE™

Selection of our books indexed in the Book Citation Index in Web of Science™ Core Collection (BKCI)

Interested in publishing with us?
Contact book.department@intechopen.com

Numbers displayed above are based on latest data collected.
For more information visit www.intechopen.com

Chapter 2

Graphene-Based Composites and Hybrids for Water Purification Applications

Rahul Sharma and Parveen Saini

Additional information is available at the end of the chapter

http://dx.doi.org/10.5772/63666

Abstract

The increasing water demand and the worldwide shortage of clean water call for new technologies for wastewater treatment, of which sorption is recognized as simplest and efficient method for all major water pollutants, including heavy metal ions, organic dyes and organic solvents. In this context, graphene, an atomically thin two-dimensional hexagonal arrays of carbon atoms, and its analogs have been visualized as ultimate materials for the separation of pollutants from water due to properties such as superhydrophobicity, superoleophilicity, chemical-environmental-thermal stability, chemical manipulability, controllable morphology, texture, porosity and accessible surface area, facile processing, low density, biocompatibility and low-cost synthesis from a variety of abundant carbonaceous precursors. This chapter begins with an introduction of water purification, related processes and fundamentals of adsorption and absorption phenomenon. The next section emphasizes the importance and advantages of graphene as sorbent, brief about its synthesis, types of graphene-based composites/hybrid systems and their synthesis strategies. The last section throws light on the performance of graphene-based foams, aerogels and composites/hybrids for the separation of metal ions, organic dyes and various oils/organic solvents, supported by comprehensive literature account. Finally, the chapter concludes with the comments on the current status, major challenges and future scope in the direction.

Keywords: sorption, adsorption, absorption, graphene oxide (GO), reduced graphene oxide (RGO), superhydrophobicity, superoleophilicity

1. Introduction

In the current scenario of global socioeconomic development, environmental conservation is a major concern and numerous initiatives have been undertaken to handle air, water, soil, noise

and electromagnetic pollutions [1–13]. In particular, water pollution is recognized as a big threat for society, and enormous efforts are underway to prevent contamination of freshwater and to purify contaminated water. The water pollution is considered as an offshoot of scientific and technological growth, industrial revolutionization and ignorance/unavailability of efficient waste management strategies. The discharge of domestic and industrial effluents/wastewater into water bodies not only makes water sources unfit for drinking purpose but also adversely affects its utility for pharmaceutical, agricultural, chemical and industrial applications. In particular, dumping of untreated wastewater at domestic and industrial levels (e.g., by paper, textile, food, leather and chemical industries) introduces hazardous substances, for example, dyes, chromium compounds, heavy metals such as copper, arsenic, lead, cadmium, mercury, nickel, cobalt and certain toxic organic chemicals, into rivers, lakes and other freshwater bodies [10,14–18]. These contaminants affect the photosynthesis in aquatic systems and disturb the self-purification mechanism [19] of water with extinction of some aquatic species as one of its worst consequence. Their acute exposure poses serious health hazards for human, for example, organic dyes and heavy metal ions are known to exert harmful effects such as an increased heart rate, vomiting, shock, cyanosis, jaundice, tissue necrosis, bone defects, renal damage, paralysis and even death [20–22] in some cases.

The leakage and spilling of industrial chemicals and oils into water bodies also disturb the water quality and adversely affect the aquatic life. The large-scale oil spill accidents (occurring during onshore/offshore handling of oils) are identified as catastrophic and devastating situation for marine life. It also adversely affects the infrastructure (e.g., beaches), underwater ecosystem (fauna and flora) and badly affects the economies in terms of losses in tourism, fishing, seafood sectors and expenditures for the restoration of the same [23–31]. Therefore, in the past half-century, an extensive research was carried out across the globe to develop a number of efficient and smart materials/technologies for the effective treatment of wastewater containing various pollutant, especially metal ions, dyes, oils and solvents [32–42,17,43–45]. Among currently available mechanical, chemical and biological water purification processes such as coagulation, flocculation, ozone treatment, chemical oxidation, membrane filtration, ion exchange, photocatalysis and sorption [46–56], sorption (adsorption-absorption) practices emerged as most preferred commercially viable solution, owing to specific advantages in terms of simplicity of process, cost-effectiveness, environmental friendliness, applicability to diversified pollutants and low-energy consumption. In particular, adsorption practices are the sole most promising alternates in the isolation of metal ions that are otherwise very difficult to remove by means of photocatalysis and membrane filtration [57,58]. However, adsorption has also been demonstrated as viable solution for the removal of hazardous organic dyes from the wastewater streams of various industries. In contrast, absorption practices are prevalent in selective removal of nonpolar (hydrophobic) pollutants such as mineral or vegetable oils, crude oils and common organic solvents [28,59,60] from their aqueous emulsion or floating layers over water.

In the past, a number of adsorbing-absorbing materials have been exploited for wastewater treatment, including zeolite [61], silica gel [62], activated alumina [63], fly ash [64], polymeric and carbon-based materials [65–68]. Among them, carbon-based systems with environmental

http://dx.doi.org/10.5772/63666

compatibility, large-scale availability, high porosity, large specific surface area and low cost are the most promising. Activated carbon derivatives with high degree of porosity and large specific surface area (600–2000) m^2g^{-1} are used in adsorption-based water purification for many years [65,69–72]. However, essentiality of their surface activation to enhance adsorption capacity and release of secondary pollutants in the form of fine particles in water limited their utility. The new members of the carbon family fullerene, carbon nanotube (CNT) and graphene have truly revolutionalized the field with graphene, the latest member of the family, seems to be most promising alternate owing to its extraordinary mechanical, thermal & chemical properties coupled with very high specific surface area, inherent hydrophobicity, tunable chemical structure, cost-effective and scalable synthesis [10,73–78]. In this context, the quest for the development of highly efficient adsorbents and absorbents and advancements in graphene science and technology fuelled numerous efforts for designing/selecting highly efficient graphene-based sorbents, understanding their pollutant-capturing mechanism and assessing their actual purification performance [16,47,57,79–83,43].

It is worth mentioning that though sorption is a broad term, the underlying adsorption and absorption subprocesses are surface- and bulk-related phenomenon, respectively, and their governing factors are entirely different. For example, adsorption process depends on parameters such as nature of adsorbent-adsorbate pair, accessible surface area of adsorbent, concentration of pollutants, temperature, pH, etc [15,45,48,84]. In contrast, absorption is regulated by pore size/volume of the sorbent, its texture and wettability characteristics along with physical attributes of absorbate species and absorbent-absorbate interfacial properties [75,85,86]. Therefore, detailed understanding of adsorption and absorption phenomenon, related terminology, important parameters and governing empirical equations is necessary before identifying and designing a suitable graphene-based adsorbent or absorbent.

2. Adsorption

The term adsorption implies the presence of an excess concentration of molecular species (gas or liquid), known as adsorbate (**Figure 1**), at the surface of porous solid (i.e., at solid-fluid interface), known as adsorbent, compared to its concentration in bulk of the adsorbent.

Adsorption arises due to the fact that the surface particles of the adsorbent are not in the same environment as the particles inside the bulk. In solids, unsatisfactory valence forces of surface

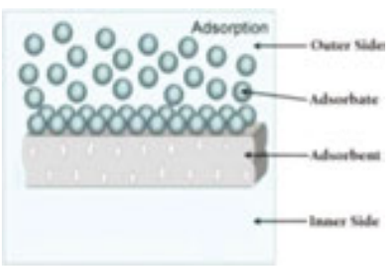

Figure 1. Pictorial representation of adsorption process.

atoms, activate the surface. At these activated surfaces, other substances stick feasibly with a decrease in the entropy (*S*) of the system. Since every spontaneous process is driven by a decrease in Gibbs free energy (*G*) that can be expressed as follows:

$$\Delta G = \Delta H\text{-}T\Delta S \tag{1}$$

Therefore, adsorption is essentially an exothermic process and the magnitude of change in enthalpy (ΔH) must be greater than the magnitude of term '$T\Delta S$'. As the adsorption proceeds, ΔH becomes less negative and ultimately becomes equal to $T\Delta S$, so that ΔG becomes zero and equilibrium is attained.

The term adsorption involves the capture of adsorbate exclusively over the surface of adsorbent. Therefore, on the basis of type interaction between adsorbent and adsorbate (i.e., physical or chemical), adsorption can be classified into two main categories, namely physisorption that involves van der Waals binding forces and chemisorption [87] wherein a strong chemical bond formation takes place between adsorbent and adsorbate. Adsorption is a complex phenomenon and requires systematic studies to understand completely its mechanism, kinetics and the thermodynamic parameters that influence adsorption capacity and rate. In particular, homogeneous and heterogeneous adsorption types have been identified with the involvement of single or multilayer adsorption of adsorbates [87]. To understand such processes and to account for the equilibrium adsorbate concentration over adsorbent and bulk of solution, several adsorption isotherms and related governing equations have been proposed, which are described in the following section.

2.1. Freundlich adsorption isotherm

Freundlich, in 1909, gave an empirical relationship between the quantity of a substance adsorbed by unit mass of solid adsorbent and the equilibrium concentration of adsorbate solution at a particular temperature for heterogeneous surfaces, which can be expressed by the following Eq. (2) [70]:

$$x / m = q_e = kC_e^{1/n} \tag{2}$$

where 'x' is amount (in mol) of adsorbate adsorbed by 'm' units amount (in g) of adsorbent. The constants K and n are the characteristics of given adsorbent-adsorbate pair. C_e is the equilibrium concentration (i.e., when adsorption is complete) of adsorbate solution. The use of logarithmic function converts Eq. (2) into the following linear form:

$$\log q_e = \log\left(x / m\right) = \log K + \frac{1}{n}\log C_e \tag{3}$$

Plot of log(x/m) versus log C_e gives a straight line and values of 'n' and 'K' can be calculated from its slope and intercept, respectively. The validity of Freundlich adsorption isotherm depends upon the completion of adsorption process. Equal volumes of standard solutions are added to equal amounts (m) of adsorbent (say charcoal) in different flasks. The final concentration (C_e) is determined in each flask after adsorption. The difference in the initial and final concentrations gives the value of 'x'. For each set of 'x' and 'C_e' values, the validity of Freundlich isotherm can be established using Eq. (3).

2.2. Langmuir adsorption isotherm

Langmuir derived a quantitative expression for variation in the extent of adsorption with concentration, by assuming the equilibrium nature of adsorption and fixed number of equivalent energy adsorbing sites on adsorbent surface [70] .This model is applicable to homogeneous surfaces and assumes that only monolayer of adsorbate molecules formed on adsorbent surface and there is no interaction between the adsorbate species after adsorption. This isotherm represents the equilibrium distribution of a material in solid and liquid or gas phases and can be mathematically expressed as follows [70]:

$$x / m = q_e = \frac{qKC_e}{1 + KC_e} \tag{4}$$

where q_e and C_e are the equilibrium adsorption capacity (mol/g) and equilibrium concentration of adsorbate solution, respectively. The constants K and q are the Langmuir's constant and maximum monolayer adsorption capacity. The linear form of Langmuir Eq. (4) is given as follows:

$$\frac{1}{q_e} = \frac{1}{q} + \frac{1}{qKC_e} \tag{5}$$

By plotting $1/q_e$ against $1/C_e$ value of K and q can be calculated from slope and intercept, respectively, of fitted straight line. In order to judge the feasibility of adsorption, a dimensionless constant parameter R_L called separation factor is defined, which is related to Langmuir constant and initial concentration C_i of adsorbate solution as follows [70]:

$$R_l = \frac{1}{1 + KC_i} \tag{6}$$

This constant explains the characteristic features of Langmuir's adsorption isotherm, as it indicates the shape of isotherm/energy of the adsorption. The magnitude of R_L signifies the feasibility of adsorption as R_L>1, R_L=1, 1<R_L>0, R_L=0 indicates unfavorability, linearity, favorability and irreversibility of adsorption, respectively [70].

2.3. Temkin adsorption isotherm

According to Temkin adsorption isotherm, energy of the adsorption is a linear function of adsorbent surface coverage by assuming the indirect interaction of adsorbent and adsorbate [18]. The heat of adsorption of adsorbate molecules decreases with increase in the surface coverage of adsorbent [18]. This model can be represented by the following mathematical equations:

$$q_e = \frac{RT}{b} \ln kC_e \tag{7}$$

$$q_e = B \ln K + B \ln C_e \tag{8}$$

where q_e is the equilibrium adsorption capacity (mol g^{-1}) and C_e is the equilibrium concentration of adsorbate solution. Plots of q_e versus C_e give a straight line whose slope provides the values of B, which is associated with energy of adsorption, and Temkin's constant K can be calculated by intercept of the line.

A number of other adsorption isotherm models, namely BET isotherms [88], Dubinin-Radushkevich isotherm [89], Toth adsorption isotherms [90] are proposed to describe the adsorption phenomenon. Since precise mechanism of adsorption in solution phases is still not known to a greater extent; therefore, a single adsorption model is not applicable universally. The validity of these models generally changes from one adsorbent-adsorbate system to another and also with pH of solution, nature of solvent, ionic strength, etc. [15,91,18]. Freundlich and Langmuir adsorption isotherms are the two very common approaches generally used in the experimental practices. Since the use of adsorption isotherm equations essentially involves the 'curve-fitting' method, the model with higher value of regression coefficient is considered to be more valid than the one with lower regression coefficient value.

2.4. Thermodynamic treatment of adsorption isotherm

Since every spontaneous process proceeds by characteristic changes in thermodynamic parameters, thermodynamic parameters, such as Gibbs free energy change (ΔG_{ads}), change in enthalpy (ΔH_{ads}) and change in entropy (ΔS_{ads}) associated with the adsorption phenomenon, provide thorough knowledge about energy changes involved in adsorption process and the other thermodynamic variables on which adsorption depends on parameters such as temperature, pressure, etc. By designing systematic experiments, we can find out the distribution coefficient K_d. More specifically, it is equilibrium constant for the distribution of adsorbate molecules in solution phase and on adsorbent surface and given by Eq. (9):

$$K_D = \frac{C_{ea}}{C_e} \tag{9}$$

http://dx.doi.org/10.5772/63666

where C_{ea} and C_e are the equilibrium concentrations of adsorbate molecules on adsorbent surface and solution respectively. Other thermodynamic properties can be deduced using the distribution coefficient K_d.

$$\Delta G_{ads} = -RT \ln K_d \tag{10}$$

$$\ln K_d = \frac{\Delta S_{ads}}{R} - \frac{\Delta H_{ads}}{RT} \tag{11}$$

The values of the ΔH_{ads} and ΔS_{ads} will be easily determined using the van't Hoff curves by plotting K_d against T^{-1} which gives a straight line. The slope and intercept of line gives ΔS_{ads} and ΔH_{ads}, respectively. The decrease in the Gibbs free energy, that is, a negative value of ΔG, is the necessity of a spontaneous process.

2.5. Kinetics of adsorption

Thermodynamics deals with spontaneity of the processes, but it does not tell about rapidity (e.g., adsorption rates) of the adsorption process and its mechanistic details. Therefore, adsorption kinetic studies are employed for better understanding of adsorption mechanism and its rate. Since adsorption in solution phase involves more than two components viz. adsorbate, solvent and adsorbent, depending upon the adsorption system, several kinetic models have been proposed.

2.5.1. Pseudofirst-order kinetic model

In 1898, Lagergren proposed the pseudofirst-order kinetic model [15,92] for the adsorption of adsorbate particles from solution by a solid adsorbent and proposed the following governing mathematical Eq. (12):

$$\log(q_e - q_t) = \log q_e - \frac{K_1 t}{2.303} \tag{12}$$

where K_1 is the pseudofirst-order rate constant, q_e and q_t are equilibrium adsorption capacity (mol/maximum adsorption capacity for a given amount of adsorbent beyond which no further adsorption can take place) and adsorption capacity (mol/g) at a given time (t), respectively. By plotting $\log(q_e - q_t)$ versus 't' and linear data fitting values of K_1 and q_e from slope intercept, respectively. It has been realized that pseudofirst-order kinetic model is generally applicable to the initial stage of the adsorption as it only account for the involvement of only two components in adsorption process that occurs in solution phase [93,94].

2.5.2. Pseudosecond-order kinetic model

A more appropriate kinetic model for solution phase adsorption process is proposed by Ho and McKay [95] who showed that the rate of adsorption depends upon the adsorption capacity of adsorbate on solid adsorbent rather than its concentration in the solution phase. Eq. (13) was proposed to investigate the kinetics [96]:

$$\frac{1}{q_t} = \frac{1}{q_e K_2} + \frac{1}{q_e} \tag{13}$$

where K_2 and q_e represent pseudo-second-order rate constant and equilibrium adsorption capacity, respectively. Again the linear fitting of 't/q_t' versus 't' plots allowed the determination of K_2 and q_e from the calculated intercept and slope values.

For a better look into the mechanistic pathways, one should accounts the three basic steps by which adsorption proceeds viz. (i) the movement of adsorbate particles through bulk solution to the external surface of adsorbent, (ii) diffusion of adsorbate particles in the pores of adsorbent (interparticle diffusion) and (iii) adsorption of the adsorbate particles on the active sites of adsorbent. Any of the above steps can be rate-determining step.

For the identification of various steps involved in the adsorption process, interparticle diffusion model is used, which is expressed as follows [97]:

$$q_t = K_i T^{1/2} + C \tag{14}$$

where K_i is the interparticle diffusion rate constant and C is a numeric constant. If interparticle diffusion is the rate-determining step of the adsorption process, then the above equation gives straight line for q_t versus $t^{1/2}$ plots.

3. Absorption

Absorption is a phenomenon in which chemical substances, such as atoms, molecules and ions, enter into the bulk phase of absorbent and distributed throughout the bulk of absorbent. The process of absorption can be either physical [98] or chemical [98] depending upon the interaction between the absorbent and the absorbing species. Physical absorption is sometimes referred as a nonreactive process, for example, the absorption of air oxygen in water at air-water interface [99]. Such absorption phenomenon is highly temperature and pressure dependent. In practice, the absorbing capacity of the absorbent depends upon the interfacial surface area, contact time and the wettability characteristics of the both substances. For example, superhydrophilic materials preferentially absorb water molecules from a mixture of several substances, whereas superhydrophobic surfaces (e.g., lotus leaf) tend to exclude water. A reactive or chemical absorption process, which takes place by means of some chemical

http://dx.doi.org/10.5772/63666

reactions, for example, the absorption of carbon dioxide by sodium hydroxide, occurs via the formation of sodium carbonate [99]. Since the absorption of adsorbate occurs through the surface of absorbent, surface properties of the solid absorbent are most critical in deciding their absorption capacity, absorption rate, etc. These properties include surface energy [100], surface wettability, [100] topological roughness [101] and contact angles [101]. For absolutely flat surfaces, surface wettability can be determined using Young's equation that correlates the interfacial surface energies with contact angle value by the following equation:

$$\cos\theta_r = \frac{\gamma_{sv} - \gamma_{sl}}{\gamma_{lv}} \tag{15}$$

where γ_{sv}, γ_{sl}, γ_{sl} are surface-free energy of involved solid-gas, solid-liquid and liquid-gas interfaces, respectively, and θ_r is the water contact angle with solid surface (**Figure 2a**). Therefore, for a solid absorbent, low surface energy is required for higher water contact angles (WCAs). Since lower contact angles are the direct reflection of surface wettability, for achieving highly wettable or superhydrophilic surfaces, we need to design the surfaces having minimum surface energies and an opposite situation is required for superhydrophobic surfaces having excellent wettability for nonpolar liquids such as oils and organic solvents. In addition to this, surface roughness and topology are another crucial factors for high/low WCAs, which are explained on the basis of Wenzel [102] (**Figure 2b**) and Cassie-Baxter [103] (**Figure 2c**) models.

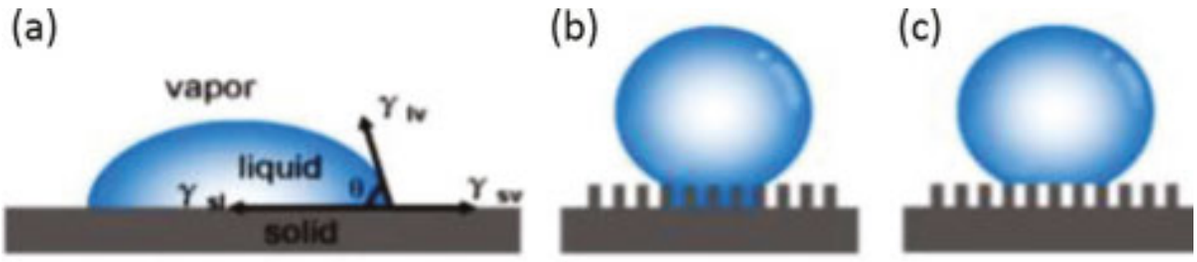

Figure 2. Schematic representation of wetting behavior of water droplet on solid absorbent (a) Young's model, (b) Wenzel model, (c) Cassie model. Reproduced from [75] with permission from RSC.

According to Wenzel's theory, no air bubbles are present between the liquid and solid surface. Hence, the liquid floods the roughness introduced channels (**Figure 2b**) leading to perfect wetting of the underlying surface, so that the contact angle of smooth (nontextured) and structured (rough) surfaces satisfy the following equation:

$$\cos\theta_\omega = \mathrm{r}\cos\theta \tag{16}$$

where θ_ω and θ are the contact angles of structured (rough surface) and smooth (nontextured) surfaces respectively, '*r*' is the roughness ratio (i.e., ratio of the true surface area of the structured surface to its projection area). The equation indicates that the surface roughness can

alter the actual wettability of the surface. If r>1, then the microstructured surface can increase the hydrophobicity (if θ>90°) and hydrophilicity (if θ<90°) of the actual smooth surface.

In Cassie's model, due to the presence of air molecules present between the surfaces of two phases (i.e., within roughness introduced channels), solid surface is not perfectly wetted by liquid (**Figure 2c**). Hence, the contact angles of structured (rough) surface (θ_c) and smooth surface (θ) are related by following equation:

$$\cos\theta_c = f_1 \cos\theta - f_2 \tag{17}$$

where f_1 and f_2 are the ratios of solid-liquid interface and solid-gas interface areas to their combined (f_1+f_2) projection area, respectively. According to the equation, the presence of air pockets between the solid and liquid surfaces leads to increase in contact angle value. In addition to absorbent properties, the absorbate's physiochemical characteristics are also crucial in determining the absorption effectiveness of the solid absorbent. Since absorption is a mass transfer phenomenon, it heavily depends upon the density and viscosity of the absorbates. Generally, less viscous liquids (low cohesive energy) tend to absorb faster compare to highly viscous liquids [104]. As the pore volume of a given absorbent is fixed, and hence, it can only absorb a fixed volume of a liquid, the absorption capacity an absorbent can be linearly related with the densities of the absorbing liquids [105].

4. Synthesis of graphene-based hybrids and composites

A number of strategies have been used for the synthesis of variety of adsorbents and absorbents constituted by graphene-based hybrids and composites.

4.1. Dip-coating process

Figure 3. Schematic representation of formation of graphene-coated absorbent sponges by dip-coating process.

The dip coating is actually a two-step process (**Figure 3**) involving coating of graphene oxide (GO) over substrate (foam/particulate-solid) followed by chemical reduction of coating to reduced GO (RGO). In the typical coating process, sponge/foam substrate is immersed inside aqueous dispersion of GO for specified time and dried to form GO-coated foam. The concentration of GO solution and number of dip-dry cycles may be varied to change the coating

http://dx.doi.org/10.5772/63666

thickness and uniformity and ultimately the GO loading. Once the desired coating/loading is achieved, the foam may be chemically reduced by exposure to chemical reducing agents such as hydrazine, ascorbic acid or other systems, resulting in the formation of RGO-coated foam. The formation of GO and RGO coatings are evident from the change in the shade of foam to brownish and blackish, respectively. The dip-coating process involved simple physical interactions between GO/RGO coating and foam and possess disadvantages in terms of coating uniformity and its poor adherence. In it modified version involving chemical grafting, suitable functionalized derivative of GO is chemically grafted over substrate (foam/particulate-solid) carrying complimentary functional groups. Such foams display better coating uniformity and adherence compared to dip-coating process.

4.2. Surface coating by *in situ* generation of graphene via thermal treatment

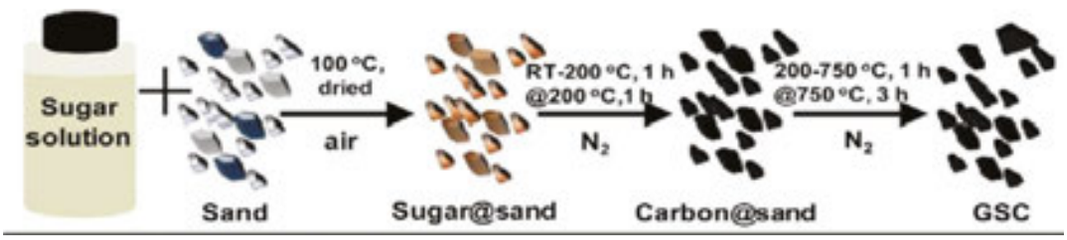

Figure 4. Schematic representation for the synthesis of graphene-coated sand composites. Reproduced from [106] with permission from ACS.

In such process, substrate material (e.g., sand) is treated with suitable (carbonizable) graphene precursor (e.g., sugar solution) leading to surface coating (**Figure 4**) with precursor (sugar with sand) upon drying. Further, high-temperature treatment leads to the carbonization of coated precursor and formation of graphene-/sand-type hybrids [106] (GSCs).

4.3. *In situ* incorporation process

In this process, the aqueous dispersion of GO (colloidal solution) is mixed with suitable secondary phase (CNTs, inorganic nanoparticles such as Fe_{23}/Fe_3O_4) and subjected to further processing to form 3D self-assembled structures and cause reduction of GO phase to RGO.

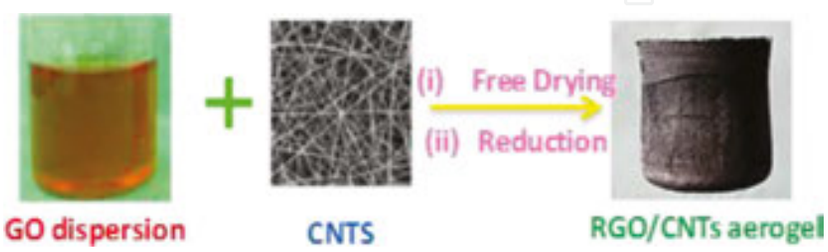

Figure 5. Schematic representation for the synthesis of a graphene composite by *in situ* incorporation of CNTs in GO solution.

For example, GO/CNTs mixed solution is subjected to freeze drying followed by chemical reduction to form RGO/CNTs hybrid-based aerogels (**Figure 5**). The presence of CNTs prevents the stacking of RGO phase and provides improved porosity and mechanical strength to the aerogel.

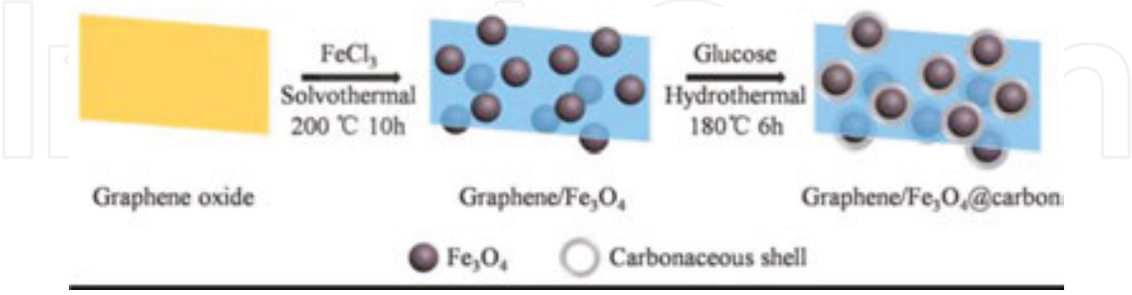

Figure 6. Schematic representation of *in situ* incorporation process involving the mixing of GO with suitable filler followed by secondary processing. Reproduced from [53] with permission from RSC.

Similarly, GO/Fe_3O_4/glucose system is hydrothermally treated at high temperature to form the RGO/Fe_3O_4-based hybrids in a single step (**Figure 6**). Here, the Fe_3O_4 phase checks the RGO agglomeration, improves porosity and allows magnetic separation of the hybrids from the water (after the completion of uptake of pollutant).

4.4. Hydrothermal process in the presence of gelation-causing agent

This involves the hydrothermal treatment of GO dispersion in the presence of suitable gelation agent, for example, chitosan leading to the formation of hydrogel [107], which may lyophilized or supercritical dried to form the corresponding hybrid aerogel.

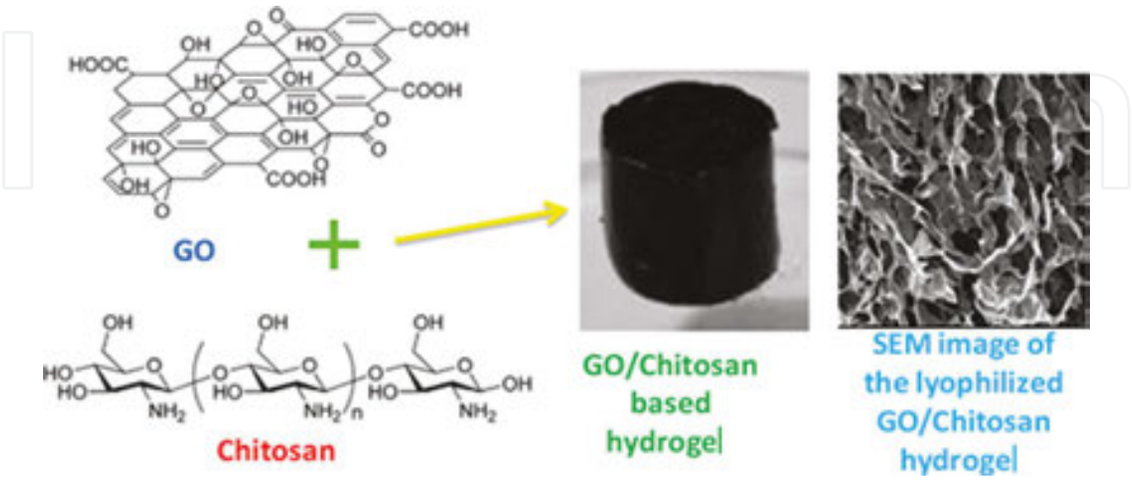

Figure 7. Photograph of GO/chitosan hydrogel and its SEM image. Reproduced from [107] with the permission from RSC.

http://dx.doi.org/10.5772/63666

For example, mixed aqueous dispersion of GO and chitosan may be hydrothermally converted into 3D self-assembled macroscopic hydrogel (**Figure 7**), which consists of highly porous structure as evident from the scanning electron microscope (SEM) investigations of its lyophilized version.

5. The water purification performance of graphene-based hybrids and composites

As already discussed in previous section, due to its high specific surface area, tunable morphological features, controllable porosity, inherent hydrophobicity and oleophilicity, chemical manipulability, tunable surface functionality, facile processing via chemical route and good thermal/environmental/chemical stability, graphene has been widely used to design variety of sorbents to selectively remove the pollutants via adsorption (e.g., for metal ions or organic dyes) or absorption (e.g., for oils or organic solvents) processes [15,17,18,43,53,79,81,91,97,105,108–111]. The contaminant capture ability, including the affinity, toward particular type of contaminant, capturing mechanism and actual purification performance of synthesized graphene-based platforms depends upon the presence of specific set of above properties. This section provides comprehensive account of the purification performance of the graphene-based hybrids and composites for three major classes of pollutants viz. metal ions, organic dyes and oils/organic solvents, with emphasis on the role of above-mentioned specific properties and their correlation to observed performance [47,52,106,112].

5.1. Adsorption of metal ions

It has been well established that the presence of excessive amounts of heavy metals such as Hg (mercury), Pb (lead), As (Arsenic), Cr (chromium), Cu (copper), Ni (nickel), Cd (Cadmium), Se (selenium), etc. in water has a catastrophic effects on living systems and as they degrade the quality of water for other practices like in industries and agricultural sector. The main sources of these metal ions in water systems include effluents of various processes such as galvanization, batteries' waste disposal, mining operations and paper/textile industries, tanneries, etc. [74,91]. Therefore, the removal of above metal ions from the wastewater streams is very important and several efforts in the direction are made using graphene-based adsorbents.

Chandra et al. synthesized magnetite (Fe_3O_4)/reduced graphene oxide (M-RGO) composites [17] and demonstrated their good binding affinity toward As(III) and As(V) ions. The presence of Fe_3O_4 phase enable easy removable of spent adsorbent from water after completion of adsorption of As ions. The composites displayed arsenic removal efficiency (>99.9%) with maximum adsorption capacity (**Figure 8b**) of 13.10 mg/g and 5.83 mg/g for As(V) and As(III), respectively.

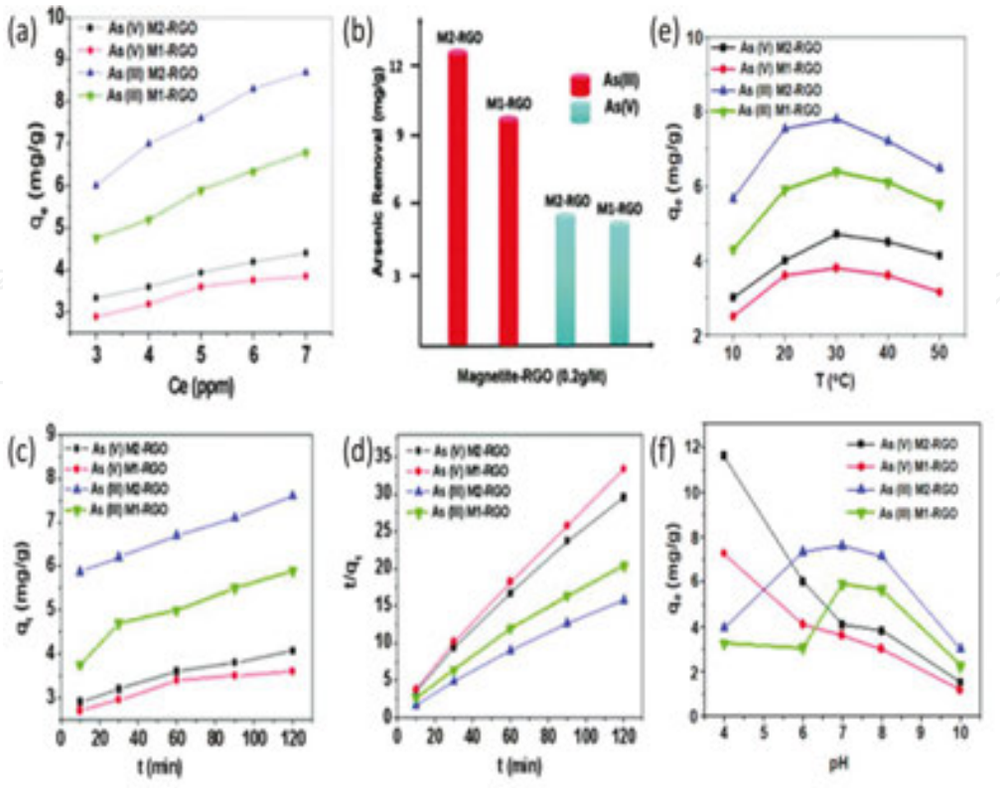

Figure 8. (a) Adsorption isotherms of As(III) and As(V) on the Fe_3O_4-RGO composite (temperature 20°C, pH 7). (b) Maximum adsorption capacity of M-RGO composites for arsenic removal from water. Kinetic absorption data plots of arsenic ions by M-RGO: (c) arsenic removal rate q_t versus time t and (d) the transformed rate plot t/q_t versus t. (e) Effect of temperature on arsenic adsorption: pH, 7; adsorption time, 2 h; adsorbent dose, 0.2 g/L; and arsenic concentration 5 ppm, (f) Effect of pH on arsenic adsorption: temperature, 20°C; adsorption time, 2 h; adsorbent dose, 0.2 g/L; and arsenic concentration, 5 ppm. Adopted from [17] with permission from ACS.

The authors plotted the adsorption isotherm (**Figure 8a**) and fitted kinetic data (**Figure 8c** and **8d**) into pseudosecond-order kinetic model and showed the applicability of the model on adsorption process. They also outlined the optimum temperature (**Figure 8e**) for maximum adsorption capacity. The difference in adsorption mechanism of As(V) and As(III) on M-RGO composites was observed by studying the effect of solution pH (**Figure 8f**) on adsorption capacity. An increase in the adsorption of As(III) (present as H_3AsO_4 arsenous acid) in basic conditions ruled out the electrostatic interactions between positively charged adsorbent and negatively charged arsenious acid. Rather, surface complexation of As(III) ions is responsible for very high adsorption capacity in alkaline conditions. On the other hand, As(V) ions present as $[H_2AsO_3]^-$ species) are electrostatically adsorbed by the adsorbent surfaces at low pH values. Wang et al. [74] exploited the surface area and charge density of graphene oxide sheets in the removal of cadmium and cobalt ions. They have studied the sorbing properties of graphene oxide nanosheets for the removal of Cd(II) and Co(II) ions from aqueous solutions at different pH values and showed that the adsorption of the Co(II) ions increases with increase in the pH of solution reaching maximum at pH>9. In case of Cd(II) ions, 98% adsorption of ions occurred at pH>9 mainly due to increase in negative surface charge density of graphene nanosheets

http://dx.doi.org/10.5772/63666

(with an increase in the pH of solution) [74], which electrostatically adsorb the positively charged metal ions. Expanding the work in this area, Fan et al. [113] fused the acid resistant, magnetic cyclodextrin with GO nanosheets (MCGN) for enhancing the adsorption capacity of the composite for Cr(VI) ions (**Figures 9** and **10**).

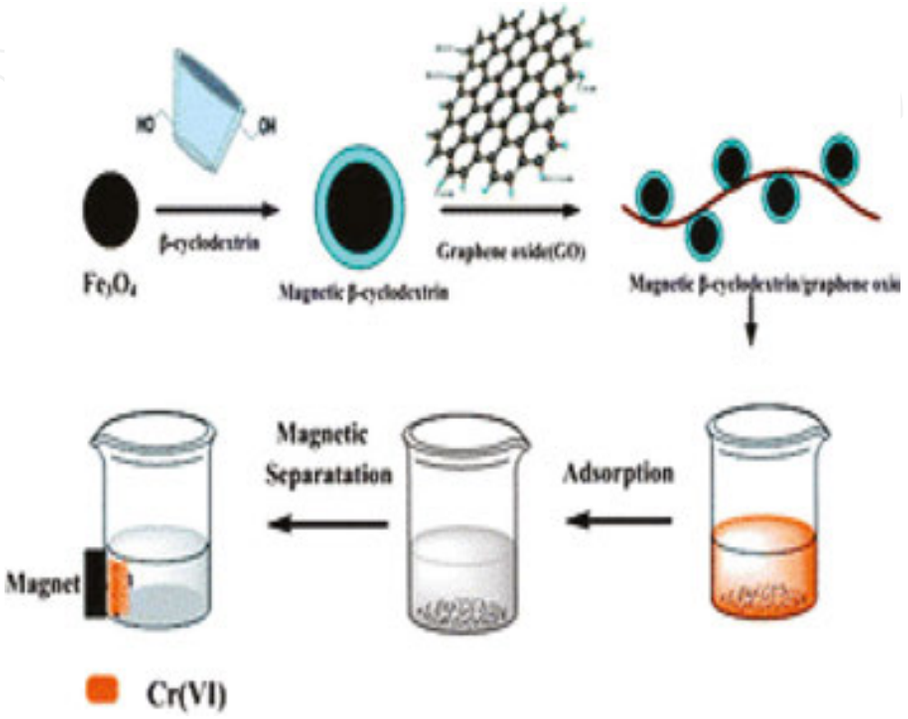

Figure 9. A schematic representation of the preparation of cyclodextrin-graphene composite and removal of Cr(VI). Reproduced from [113] with permission from RSC.

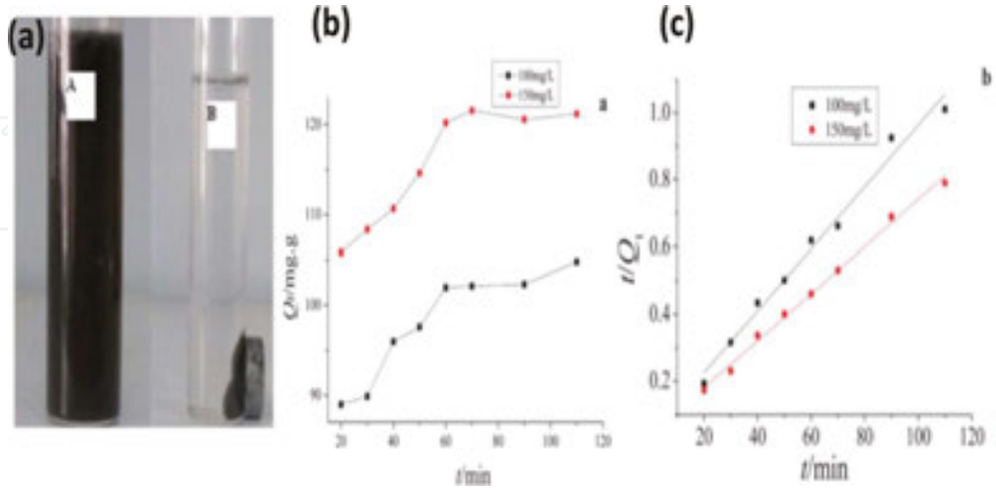

Figure 10. (a) MCGN in the absence (A) and presence (B) of external magnetic field (b) time profile and (c) Kinetics of Cr(VI) ions removal with 1 g/L MCGN concentration and initial Cr(VI) concentrations are 100 mg/L and 150 mg/L. Reproduced from [113] with the permission from RSC.

The adsorbents work better under slightly acidic conditions with good recyclability, making it a good choice for heavy metal ions removal as shown in **Figure 11**.

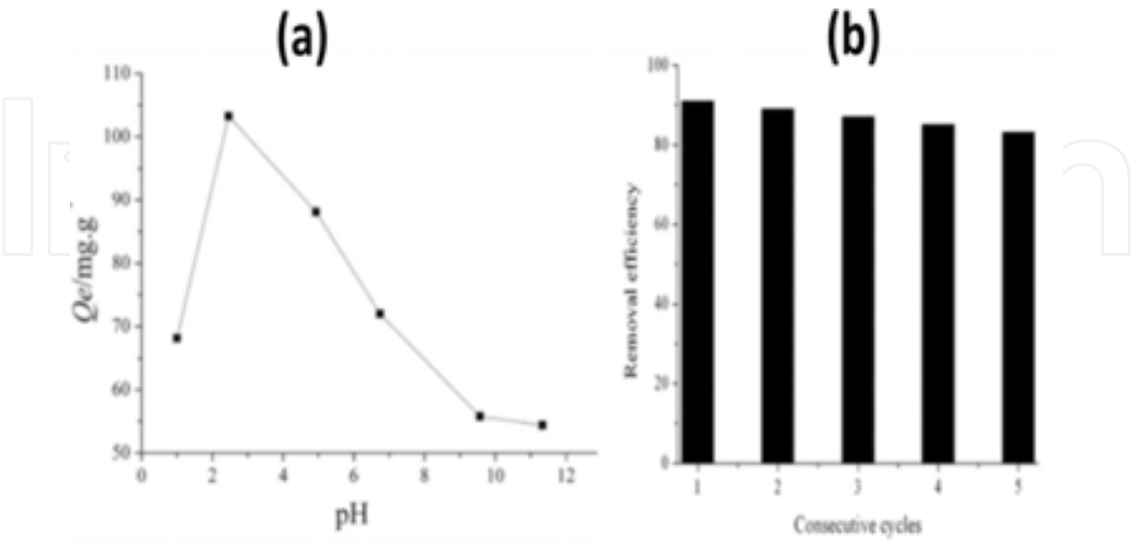

Figure 11. (a) Effect of pH on adsorption capacity of cyclodextrin-graphene nanocomposite. ([CGN] = 1 gL^{-1}, [Cr(VI)] = 100 mgL^{-1}, contact time: 60 min). (b) Recyclability of the cyclodextrin/graphene. Reproduced from [113] with the permission from RSC.

The selectivity of adsorbent for a specific adsorbate is highly desirable. Hao et al. [114] synthesized a SiO_2-graphene composite and specifically adsorb Pb(II) ions from solution. The authors observed that adsorption capacity is highly dependent on the ionic strength of solution and decrease with ionic strength due to completion between various ions for adsorbing sites. Luo et al. [82] highlighted the performance of heavy metal salts such as ZrO_2 hybridized with graphene oxide for the removal of As(III) and As(V) ions. This composite showed ionic strength independent adsorption behavior with high adsorption capacities of 95.15 mg/g and 84.89 mg/g for As(III) and As(v) ions, respectively, with good recyclability. Ren et al. [81] outlined the role of temperature of solution in regulating adsorption. The graphene-MnO_2 composite prepared by them for the removal of Ni(II) ions increase its adsorption capacity by a factor of 0.7 upon changing temperature from 298 K to 318 K. The kinetic parameters obtained from **Table 1** suggested that the pseudosecond-order kinetic model is more appropriate than pseudofirst-order kinetic model. Langmuir adsorption isotherms parameters are given in **Table 2** at various temperatures, which shows the increase in adsorption capacity at higher temperatures.

Adsorbents	**(q_e)exp (mg g^{-1})**	**Pseudofirst-order equation**			**Pseudosecond-order equation**		
		(q_e)cal (mg g^{-1})	K_1 (min^{-1})	R^2	(q_e)cal (mg g^{-1})	K_2 (g $mg^{-1}min^{-1}$)	R^2
GNS/MnO_2	42.855	28.372	0.00072	0.8672	46.447	0.00149	0.9993

Table 1. The kinetics constants of the Ni (II) adsorption onto GNS/MnO_2 composite.

http://dx.doi.org/10.5772/63666

Temperature (*K*)	GNS/MnO_2		
	q_{max} (mg g^{-1})	K_L (L mg^{-1})	R^2
298	46.55	0.333	0.995
308	60.31	0.310	0.991
318	66.01	0.558	0.999

Table 2. The Langmuir isotherm parameters of the Ni (II) adsorption onto GNS-MnO_2 composite at various temperature (*K*).

A systematic study was done by Liu et al. [45] for the adsorption of Co(II) ions on magnetite-graphene composite (**Figure 12**).

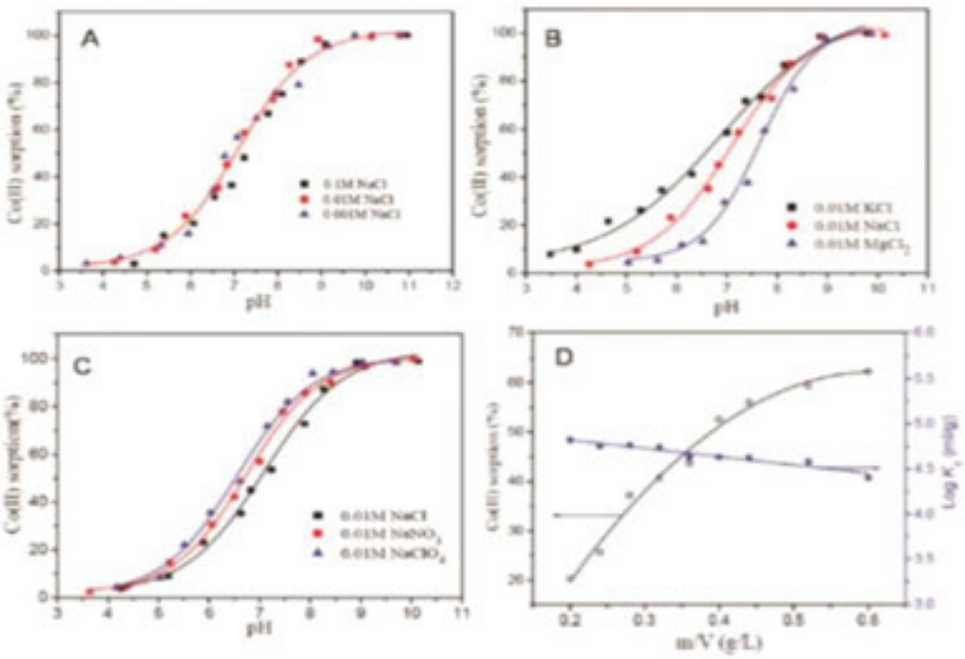

Figure 12. Effect of ionic strength (A), foreign cations (B), foreign anions (C), and sorbent content (D) on Co(II) sorption onto the M-GO composite at pH=6.8, *T*=303.15 K, *I*=0.01 M NaCl, concentration of cobalt = 10.0 mg/L from [45] with the permission from ACS.

The effect of ionic strength on adsorption capacity is negligible as shown in **Figure 12a**. But the presence of foreign ions significantly affected the adsorption behavior of the adsorbent. The pH of solution higher than 8.5 was favorable of maximum adsorption capacity. Zhou et al. [79] also reported the dependence of adsorption capacity of graphene composites on pH of solution. The material showed decreased affinity for Cr(IV) ions at higher pH as hydroxyl ion compete with the CrO_4^{2-} ions for adsorbing sites [5]. Such studies are also reported by other groups to show how metal ion compete for adsorbing sites in the environment of excessive hydroxyl ions and hydronium ions [115]. It can be concluded from the discussion earlier that graphene-based materials are highly promising for the removal of heavy metal ions from wastewater systems.

5.2 Adsorption of dyes

Synthetic organic dyes that represent important color imparting ingredient of leather, paper, textile and rubber industries are also present in significant amount in their wastewater streams [22]. These dye stuffs have serious health hazards for both humans and aquatic systems [21,116]. In recent times, graphene analogs, including GO- or RGO-based sponges, composites and hybrids, have been successfully employed for the removal of toxic dyes from wastewater.

Liu et al. [47] used a centrifugal evaporator (**Figure 13a**) to synthesize GO-based sponge (**Figure 13b**) consisting of 3D interconnected network of graphene layers and demonstrated their potential for the removal of cationic dyes such as methylene blue (MB) and methyl violet (MV) with removal efficiency of 99.1 and 98.8%, respectively, with equilibrium reaching within 2 min. It has been highlighted that the microporous structure of GO sponge (**Figure 13c**), high negative charge density (due to rich oxygen functionalities) mediated cation-anion-type interactions, π-π stacking interactions between dye backbone and adsorbent and high specific surface area (|48.4 m^2/g), collectively contribute toward the excellent dye adsorption capacity (**Figure 13d**), that is, 397 mg/g and 467 mg/g for MB and MV, respectively (**Figure 13**).

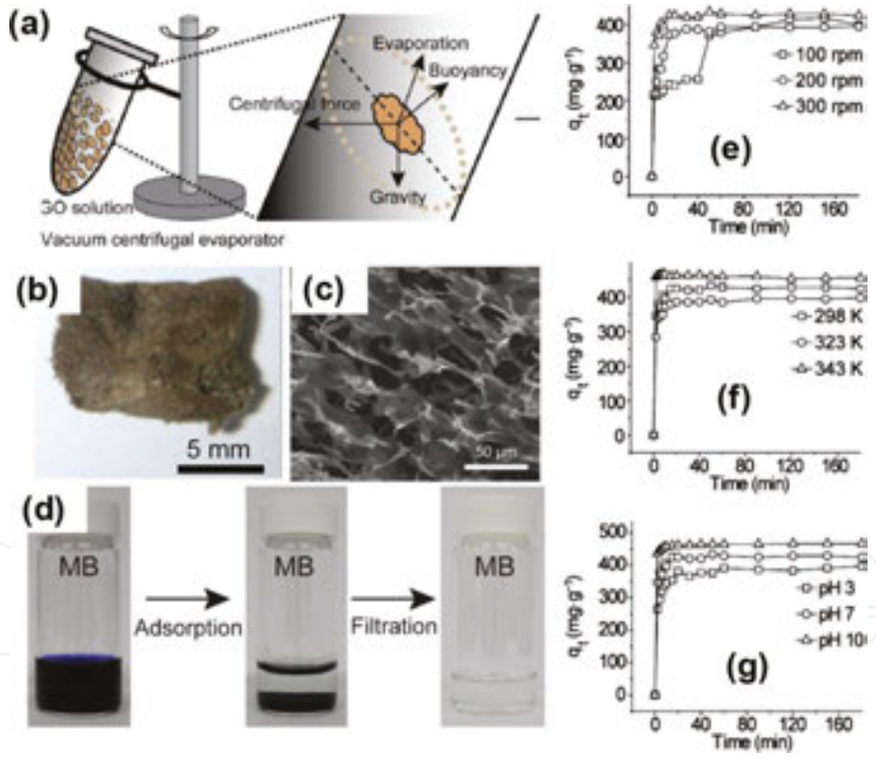

Figure 13. (a) Synthetic scheme of a 3D GO sponge, (b) optical image of GO sponge, (c) SEM image of GO sponge, (d) digital images of the original MB dye solution (left), the pale color solution with precipitated MB-adsorbed GO sponges (middle), and the colorless water after filtering the MB adsorbed GO sponge (right). Effect of (e) stirring rate, (f) temperature and (g) pH on the adsorption rate and capacity for MV dye. Reprinted from [47] with permission from ACS.

The effect of stirring (**Figure 13e**), temperature (**Figure 13f**) and pH (**Figure 13g**) on the adsorption rate and capacity have also been investigated, with the observation of increase in

http://dx.doi.org/10.5772/63666

these parameters favoring adsorption rate and capacity. Once the adsorption is complete, spent adsorbent has to be removed from purified water by filtration process, which is not only bit cumbersome but also involve risks of recontamination. Gupta et al. [106] prepared sugar-derived graphene sand composite (GSC) consisting of graphene-coated sand particles (**Figure 14a** and **b**) via thermal processing. This cost-effective active adsorbent material-packed column (**Figure 14c**) showed good R6G dye removal efficiency with adsorption capacity of 50–55 mg/g. The time-dependent adsorption studies were also carried out to understand the system kinetics (**Figure 14**).

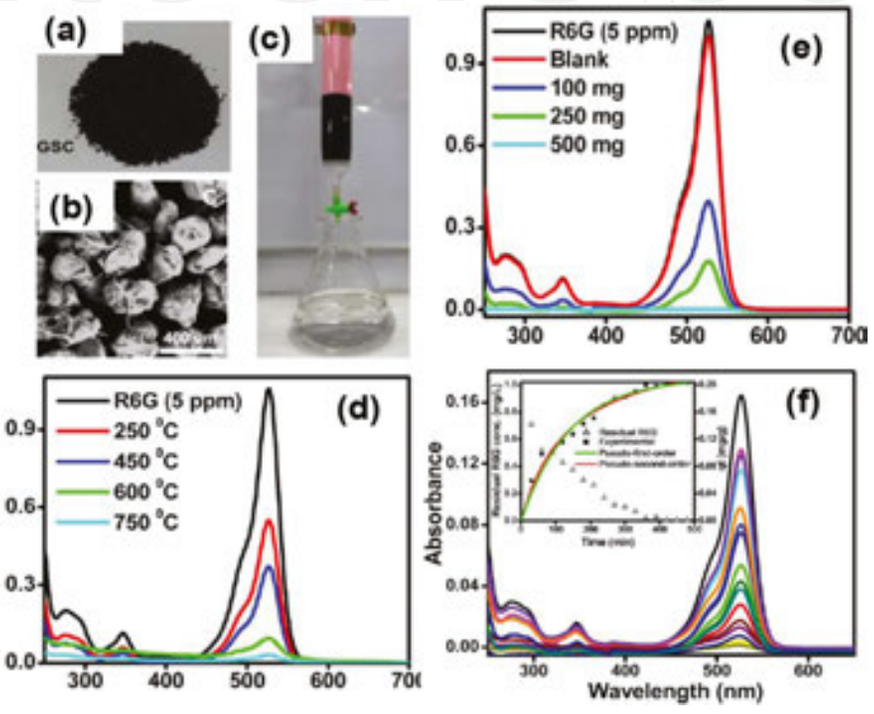

Figure 14. (a) Digital image and (b) SEM image of GSC, (c) photograph of GSC750 packed adsorption column for the separation of R6G dye. Variation of adsorption capacity as a function of (d) GSC heating temperature and (e) GSC content. (f) Kinetic study of dye adsorption with 30-min time interval. Inset shows the pseudofirst- and pseudosecond-order model fits. Reproduced from [106] with permission from ACS.

The authors highlighted the dependence of adsorption characteristics on GSC-heating temperature (**Figure 14d**) and adsorbent content (**Figure 14e**). The kinetic data were examined in terms of Lagergren pseudofirst-order (Section 2.5.1) and Ho's pseudosecond-order (Section 2.5.2) kinetic models [95] and the fitted data (inset of **Figure 14f**) showed that a pseudosecond-order equation is more appropriate in describing the experimental data. Li et al. [84] synthesized a $Mg(OH)_2$-RGO composite(GMC) to improve the adsorption capacity by increasing the porosity of the adsorbent. They pointed that surface charge density and π conjugation play an important role for high removal efficiency of GMC for cationic dyes such as MB. The presence of $Mg(OH)_2$ ensured the formation of mesoporous structure (**Figure 15** calculation of BET surface area and pore size distribution) and inhibit restacking of graphene sheets, thereby generating high accessible surface area (|104 m^2/g) for adsorption (**Figure 15**).

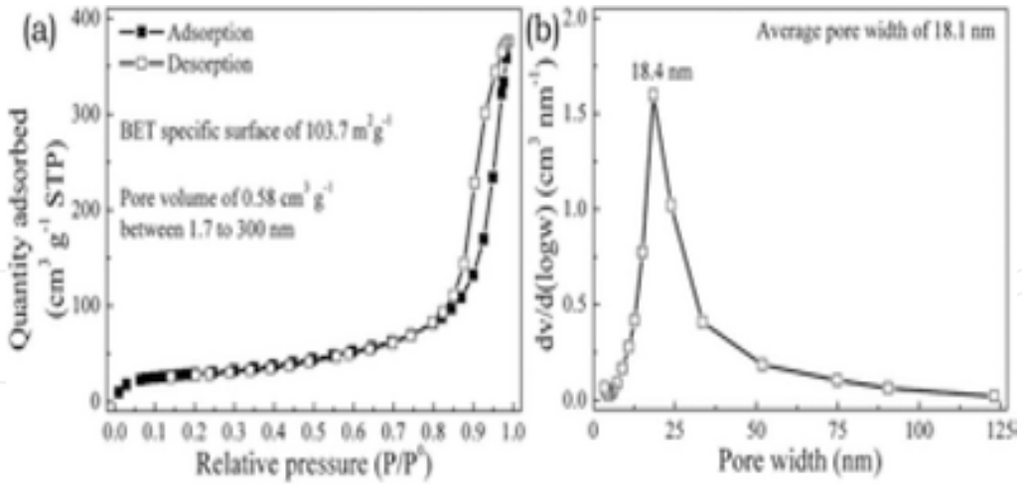

Figure 15. (a) N_2 adsorption-desorption isotherm at 77 K and (b) pore width distribution of MGC. Adopted from [84] with permission from RSC.

These GMC readily desorbs the MB molecules in ethanol solution reflecting promising recyclability. It has been observed that despite their good adsorption capacity, the separation of these graphene-based powdered adsorbents is a difficult and cumbersome task. Therefore, they pose inherent disadvantages in terms of requirement of energy-intensive separation and regeneration techniques along with chances of recontamination of water with any leftover adsorbent particles. In order to overcome poor separation ability of powdered absorbents, Fan et al. [53] synthesized graphene-Fe_3O_4 with carbon (GFC)-type hybrid materials with coupled porosity and magnetic properties for MB removal (**Figure 16**).

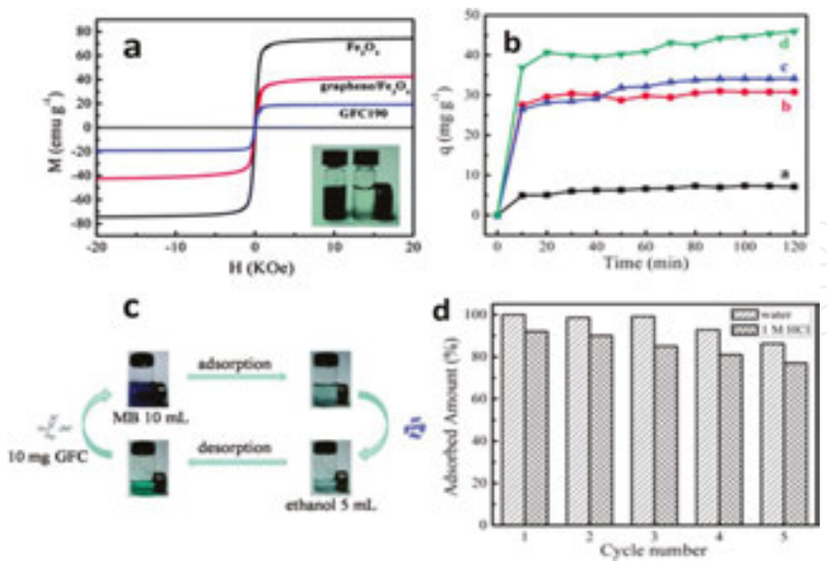

Figure 16. (a) Magnetic hysteresis loops for pure Fe_3O_4, graphene-Fe_3O_4 and GFC hybrids, (b) adsorption curves for pure Fe_3O_4, graphene-Fe_3O_4, Fe_3O_4@carbon hybrid, GFC hybrid, (c) schematic representation of recyclability of GFC hybrid, and (d) percentage removal of MB by GFC hybrid in water and 1 M HCl solution in five cycles. Reproduced from [53] with permission from RSC.

http://dx.doi.org/10.5772/63666

This material exhibits good porosity and magnetic character (**Figure 16a**) resulting in good dye adsorption response (**Figure 16b**) with good capacity (73.26 mg/g) and fast adsorption rates (i.e. removal of 80% dye within 20 min). The superiority of such materials lies in the fact that they can be easily separated after adsorption of dye from water using an external magnetic field and can be regenerated by desorbing the dye in ethanol (**Figure 16c**). The good recyclability is evident from very low decrease in adsorption capacity after five cycles of regeneration and reuse. The adsorption mechanism of MB on GFCs was examined by applying Langmuir and Freundlich isotherm models and their parameters are reported in **Table 3**.

Langmuir				**Freundlich**		
Adsorbent	q_{max} **(mg g^{-1})**	b **(L mg^{-1})**	R^2	K	N	R^2
GFC190	73.26	0.58	0.96	31.74	3.66	0.92

Table 3. Langmuir and Freundlich parameters for the adsorption of MB on GFC hybrid.

On the basis of regression coefficient (R^2) values, Freundlich adsorption is ruled out and result better fits into the Langmuir adsorption model. The good value of obtained maximum adsorption capacity (i.e., 73.26 mg/g) has been ascribed to high surface area of GFCs, which enhances the accessibility of diffusion pathways for dye molecules in macroporous domains. Additionally, strong electrostatic interactions and π-π interactions between the aromatic cationic dye and negatively charged GFC hybrid are mainly responsible for rapid adsorption rates. Wang et al. [108] also synthesized a Fe_3O_4 -graphene-based magnetic composite for the removal of fuchsine dye and showed an excellent adsorption capacity of 89.4 mg/g in very shorter time period. The kinetics of adsorption was determined by fitting the results to (**Figure 17a**) pseudosecond-order kinetic model (Eq. (13)). The regression coefficient value of 0.9999 shows the applicability of the model and confirmed the chemisorption of dye molecules on adsorbent surface (**Figure 17**).

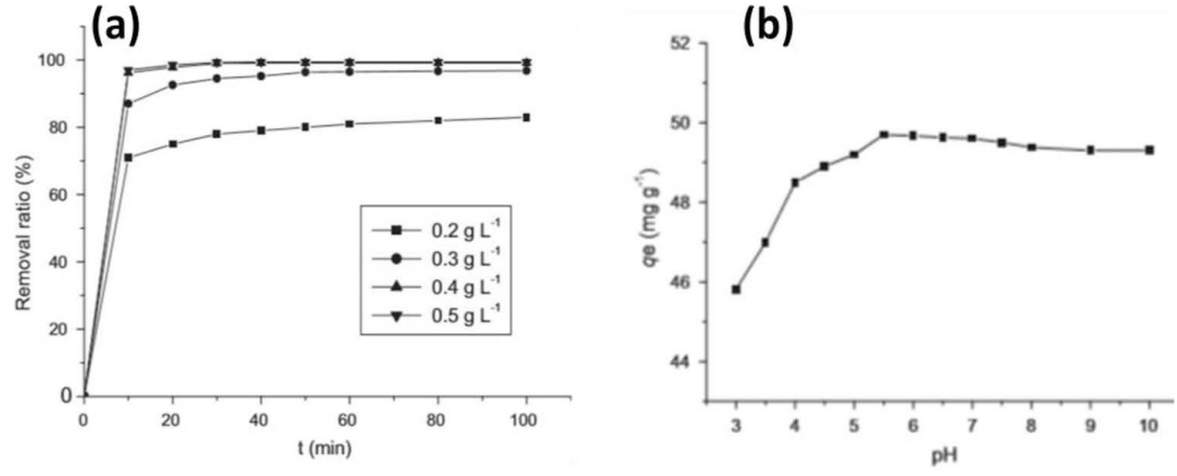

Figure 17. (a) Effect of adsorbent dose on removal ratio of dye in water and (b) effect of pH on removal of dye. Adopted from [108] with permission from Elsevier.

The authors also studied the role of dye solution pH (**Figure 17b**) on the adsorption mechanism of the composite. The adsorption capacity was found to increase with pH (from 3 to 5.5) mainly due to the fact that at low pH condition protonation of basic dye (amido groups) fuchsine occurs, which leads to increase solubility of dye in water and hence its relatively poor adsorption under slightly acidic conditions. The extensive research on development of such handy magnetic graphene materials is now of great interest as these materials have high dye removal efficiency, quick dye adsorption and facile removal of spent adsorbent from purified water after completion of pollutant adsorption. In this series, a very promising magnetic adsorbent Ni-RGO (NGC) composite is prepared by Li group [117], which almost completely removes rhodamine (RhB) and MB dyes from water within 4 h as evident from corresponding time-dependent UV-visible spectra (**Figure 18**) (**Table 4**).

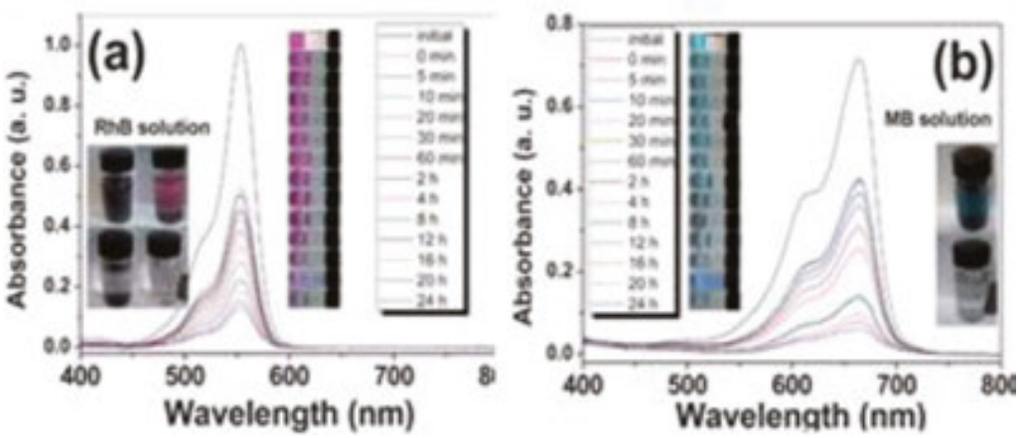

Figure 18. UV-visible spectra of original and NGC treated 50 mg organic dye solutions (a) RhB 1 × 10^{-5} M, 20 mL (b) 2 × 10^{-5}M, 20 mL for various time intervals. The insets are photographs of corresponding solutions at various time intervals and magnetic separation. Reproduced from [117] with the permission from RSC.

Constant	RhB	MB
K	0.376	0.302
N	1.048	0.894
R^2	0.99	0.99

Table 4. Freundlich isotherm constants and their correlation coefficients.

The authors show that the Freundlich adsorption mode is applicable to NGC with regression coefficient value (R^2) of 0.99 for both RhB and MB dyes, which indicates the heterogeneity of adsorbent surface. The Freundlich exponent (*n*) for RhB (1.048) is greater compared to MB (0.894) that shows the better interaction of the RhB dye with adsorbent compared to MB. This is mainly due to molecular structural differences between the two dyes. In particular, MB has a soft S-based cationic system and RhB has a hard N-based cationic system, resulting in high affinity of latter for a hard O-based anionic center. Jiang et al. [110] synthesized a magnetic

http://dx.doi.org/10.5772/63666

chitosan-graphene oxide (MCGO) nanocomposite for the adsorption of anionic dye methyl orange (MO). The magnetic adsorbent showed extraordinary MO adsorption capacity (398.08 mg/g) and easily separated by magnetic assistance after completion of dye adsorption **Figure 19a**.

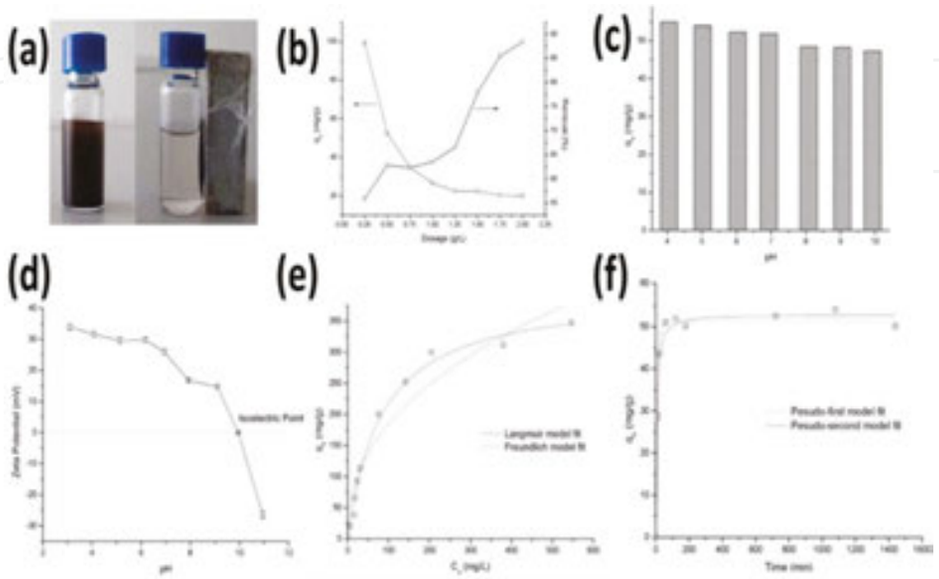

Figure 19. (a) Digital photograph of MO adsorption on MCGO nanocomposite and its magnetic separation. Variation in adsorption capacity with (b) adsorbent mass and (c) solution pH. Effect of (d) pH on zeta potential of the MCGO nanocomposite, (e) Experimental data and curve fits for Langmuir and Freundlich isotherms (f) contact time on MO adsorption by MCGO nanocomposite. Reproduced from [110] with permission from International Journal of Biological Macromolecules.

The authors showed that in case of MO, adsorption capacity decreases with pH of solution as the negatively charged MO molecules compete with hydroxide ions in alkaline conditions shown in **Figure 19c**. Also, zeta potential measurement **Figure 19d** showed that the MCGO nanocomposite attained isoelectric point at pH 10 and hence has poor affinity for anionic dye under high alkaline conditions. Because of high concentration gradient between adsorbate and adsorbent species, rapid dye adsorption takes place initially followed by a gradual decrease in adsorption rate (**Figure 19f**) as at this stage most of the adsorption sites are occupied by the dye molecules. The model fits of Langmuir and Freundlich isotherms for MO are shown in **Figure 19e**. It was found that the Langmuir isotherm better described the adsorption of MO with the higher regression coefficient R^2 (0.9897) than Freundlich isotherm (R^2=0.9112). The kinetic study concluded the applicability of the pseudosecond-order kinetic model for dye adsorption over pseudofirst-order kinetic equation and curve fitting of the experimental data for the two models is shown in **Figure 19f**.

5.3. Absorption of oils/organic solvents

Addressing the severe water pollution arising from oil spillage and chemical leakage is a challenging task. In principle, materials with both superhydrophobic and superoleophilic

properties are highly desired for solving the environmental issues because of their capacity of selective absorption of oils and organic solvents while repelling water completely. As a remediation of accidents, the cleanup of leaked chemicals or oil is a global environment issue. Generally, porous materials that have high porosity and high surface areas show great potential in oil/chemicals pickup; however, these materials usually show poor selectivity toward target oil, thus easily saturated with water. Recently, graphene-based 3D porous structures, possessing superhydrophobic and superoleophilic surfaces, attracted enormous attention owing to their high affinity for various oils and organic solvents and ability to selectively absorb them from their dispersion, emulsions or floating layered system with water. In particular, some work has been done in the direction of graphene-coated polymeric foams [105] type hybrids and graphene/composites based aerogels [118]. A number of polymeric foam substrates have been exploited for coating/decoration with graphene, including polyurethane (PU), polydimethoxysiloxane (PDMS) and melamine foams.

Liu et al. [105] fabricated reduced graphene oxide-coated polyurethane sponges (rGPU) via a two-step process involving dip coating with GO followed by its chemical reduction to RGO. In this system, porous structure of PU sponge-based substrate (SEM image **Figure 20a**) is coated with RGO layers (SEM image **Figure 20b**) without disturbance of macroporous cellular architecture of the sponge. However, due to its inherent hydrophobic nature, the uniformly coated of RGO impart high degree of hydrophobicity and oleophilicity to PU sponges, as confirmed from the contact angle measurements for water (**Figure 20c**) and oil (**Figure 20d**).

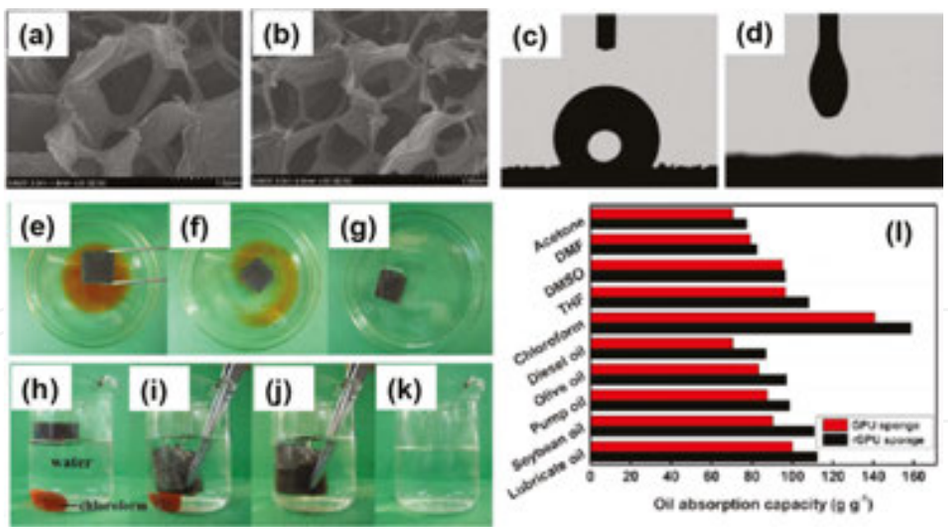

Figure 20. (a, b) SEM images of RGPU and (c, d) optical image of a water drop and lubricating oil drop on RGPU surface. Digital images of oil (e–g) and chloroform (h–k) absorption. Absorption capacity of RGPU sponge for various oils. Reproduced from [105] with the permission from ACS.

Such a combination of macroporosity, hydrophobicity and oleophilicity of these materials leads to efficient absorption of lubricating oil (**Figure 20e–g**), chloroform (**Figure 20h–k**) and variety of other oils and organic solvents with good specific absorption capacity.

http://dx.doi.org/10.5772/63666

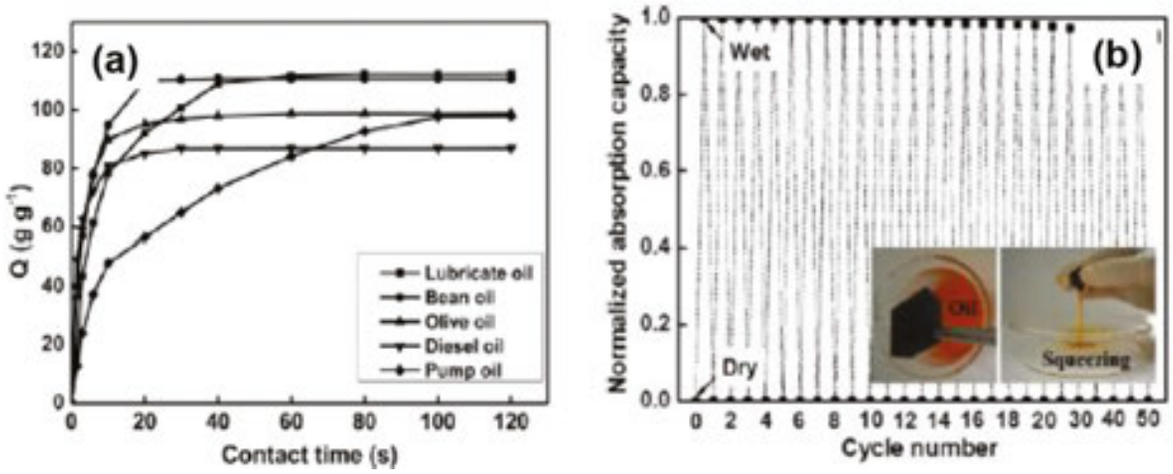

Figure 21. (a) Absorption capacities of RGPU sponge with contact time with various oils and (b) recyclability of RGPU sponge. Reproduced from [105] with the permission from ACS.

In addition, these hybrid sponges also display high absorption rate (**Figure 21a**) with saturation attaining in 2 h, The authors also exploited the compressible nature of PU sponge for the reusability of these materials and shown that they can be reused number of times (**Figure 21b**) without much loss in absorption capacity.

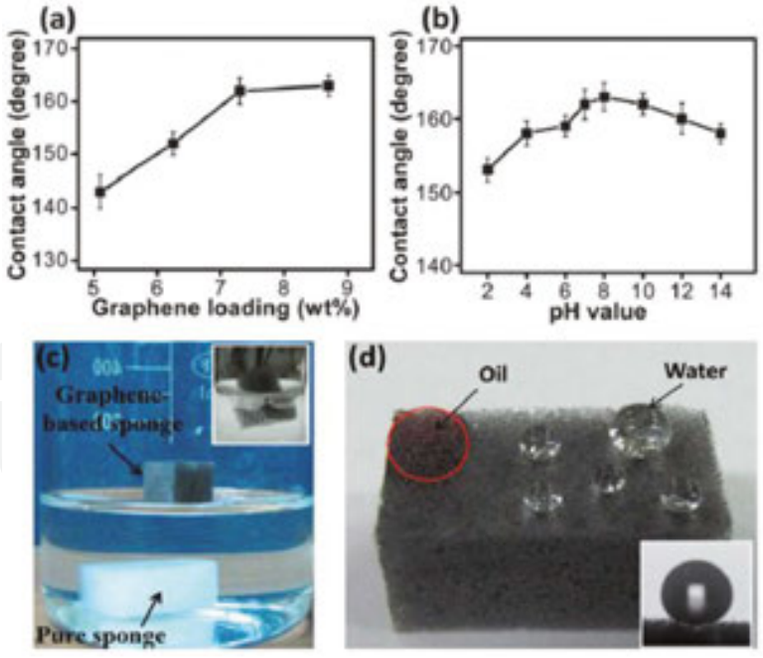

Figure 22. Effect of graphene loading on the water CA of the pure sponge (a). Relationship between pH values and CAs of the graphene-based sponges after 12 h floating on aqueous solutions with different pH values (b). Photograph of pure (white color) and graphene-based (black color) sponges after being placed on water, the inset is a photograph of the graphene-based sponge partially immersed in water by a force (c). Water droplets as quasi-spheres and motor oil trace on the surface of the graphene-based sponge (d), the inset in (d) is an optical image of a water droplet at a CA of 162. Reproduced from [86] with permission from RSC.

Nguyen group prepared graphene-coated melamine sponges [86] and highlighted the role of graphene loading and solution pH on the water contact angle value of synthesized hybrid foams. The presence of graphene nanolayers on the surface of melamine sponge drastically changed its surface properties attributed by the fact that the water contact angle changed from 0° (for pristine melamine sponge) to 162° (for graphene-coated melamine sponge). Further, the stability of superhydrophibicity to aggressive environment is demonstrated by the fact that the WCA remained greater than 150 degree even after 12 h of floating over aqueous solutions of different pH values. The pure sink to the bottom (**Figure 22c**), whereas the graphene-coated sponge floats over water, retard forced immersion with no water uptake, which further demonstrates its superhydrophobic nature. The silver mirror-like appearance of the immersed part of the graphene-based sponge (the inset **Figure 22c**) is attributed to a uniform air layer trapped between the water and superhydrophobic surfaces, which are referred to nonwetting Cassie-Baxter surfaces (Section 3). Interestingly, the sponge also displays superoleophilicity such that water droplets (pointed arrows) display WCA of 162° (inset **Figure 22d**) and remained unabsorbed (**Figure 22d**), whereas motor oil droplet (encircled) was immediately absorbed. The coexistence of superhydrophobic and superoleophilic surfaces is attributed to the combination of the microporous structure (with trapped air pockets) of the melamine sponge substrate and the hydrophobicity of the graphene nanosheets, and the micro-/nanotextured structure of graphene nanosheets on sponge skeletons.

These hybrid sponges display good absorption capacities (ranging from 60 to 165 times of its own weight) for motor oil (**Figure 23a**), chloroform (**Figure 23b**) and several other solvents (**Figure 23c**), good recyclability, low density and chemical inertness.

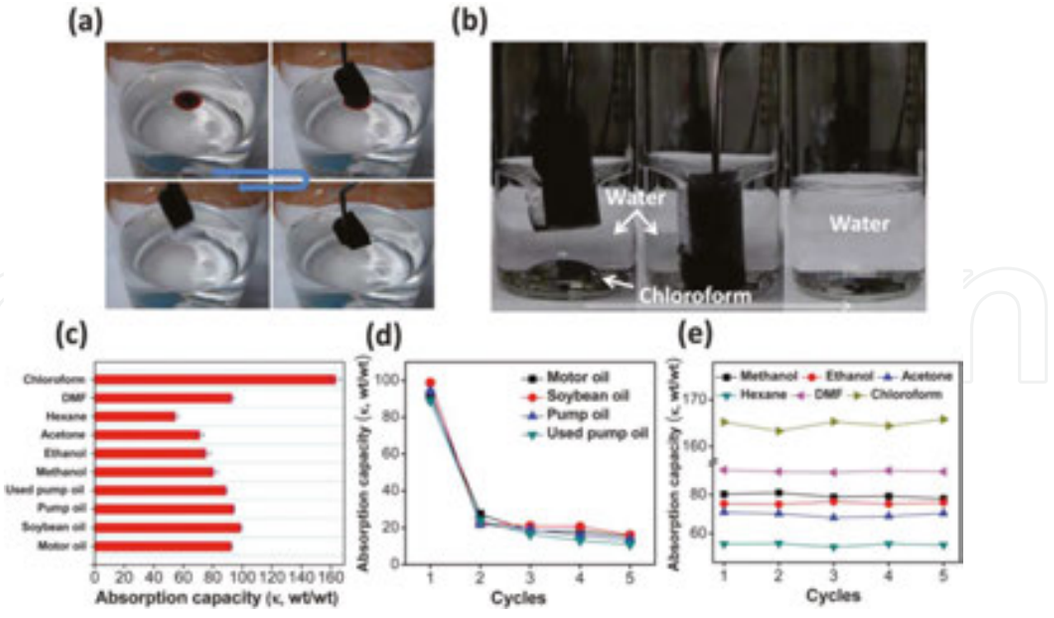

Figure 23. Snapshots of the removal process of motor oil (dyed with solvent red 24 for clear observation) (a) and chloroform (b) from water using the graphene-based sponges. Oil and organic solvent absorption capacities of the graphene-based sponges (c). Absorption recyclability of the graphene-based sponges for oils (d) and organic solvents (e). Reprinted from [86] with permission from RSC.

http://dx.doi.org/10.5772/63666

The recyclability and reusability of the graphene-based sponge also plays an important role in oil/chemical clean up applications. In general, sponge regeneration and absorbed pollutant separation can be realized either by squeezing the sponges for high-boiling materials like oils or by distillation/squeezing for low-boiling oils/solvents. It is observed that the generalized recyclable absorption response is similar for all tested oils (**Figure 23d**) with large decrease in absorption capacity after first cycle due to the residual oils inside the sponges, which cannot be removed by manual squeezing. After the second cycle, the saturated absorption capacity decreases only slightly indicating good recyclability. However, in case of organic solvents, desorbed sponges (after distillation) display no obvious change in saturated absorption capacity (**Figure 23e**) reflecting complete pollutant (solvent) recovery and good sponge recyclability, which are requisite for practical utility. Despite their great promise for oil/chemical clean up, the poor adhesion between coated graphene and foam substrate, remained a problematic issue. An attempt has been made by Tajendra et al. to improve the adhesive forces between PU sponges and RGO via covalent bonding strategy [119] involving use of silane- or titanate-based coupling agents. The sponges exhibited absorption capacity of 30–50 g/g depending upon the nature of oil/solvent. Further, the authors reported that the covalent bonding between RGO and PU prevents the leaching problem of surface layers and hence increase the recyclability of the hybrid sponges.

Table 5 compares the oil/organic-solvent removal performance of various graphene-coated foams based hybrids. It can be seen that the achieved absorption capacities are still lower than theoretically possible values and there is large deviation between results of different works. Further, besides hydrophobicity of the hybrid sponges, the parameters like viscosity, densities, polarities, surface tensions/energies of spilled chemicals and pore size, porosity and surface texturing of the foamed substrates, plays an important role in governing absorption characteristics (absorption capacity, absorption rate, selectivity) and need to be looked into thoroughly to further understanding and improvements. The graphene coating's adherence issues are sorted out to improve the reusability and to reduce the chances of cross contamination. In order to drastically improve the gravimetric absorption capacities, eliminate the adherence issues and improve the recyclability, all graphene-based 3D self-assembled networks such as graphene aerogel seems to be promising solution [16,75].

S. No.	Absorbate	Absorption capacities (g/g) of various materials			
		Graphene-coated melamine sponge	GO-coated PU sponges	RGO-coated PU sponges	TTEAI-RGO sponge
1	Chloroform	165	140	160	35
2	DMF	100	78	82	–
3	Hexane	60	–	–	–
4	Acetone	75	75	80	32
5	Ethanol	78	–	–	–

S. No.	Absorbate	Absorption capacities (g/g) of various materials			
		Graphene-coated melamine sponge	GO-coated PU sponges	RGO-coated PU sponges	TTEAI-RGO sponge
6	Used pump oil	90	–	–	–
7	Methanol	80	–	–	–
8	Pump oil	95	90	100	28
9	Soya bean oil	100	92	110	–
10	Motor oil	90	–	–	–
11	Diesel oil	–	75	90	–
12	Olive oil	–	85	100	–
13	Lubricate oil	–	100	112	–
14	Gasoline oil				45
Ref.		[103]	[63]	[63]	[104]

PU—polyurethane sponges, TTEAI— titanium (IV)(triethanolaminato) isopropoxide.

Table 5. Absorption capacities (g/g) of graphene-based materials for various oils/organic solvents.

Nevertheless, huge efforts in the direction are needed for the realization of efficient, stable, cost-effective and commercially viable absorbents for large-scale oil/chemical clean up to be used at actual spill site especially under marine environment.

7. Conclusion

In summary, graphene-based composites/hybrids have a tremendous potential for water purification applications. The inherent properties of graphene in conjunction with other materials induce additional functionalities in the composites/hybrids reflected in terms of enhanced, surface areas, porosity, flexibility, induced magnetism, improved adsorption/absorption rates and capacities. As discussed in this chapter, these materials show extraordinary chemical stabilities with good recyclability and durability, which are some of the most crucial attributes of sorbing materials. Importantly, the generation of magnetism in graphene composites/hybrids with magnetic nanomaterials prevents to ease out the sorbent operationality and its recovery process. But issues, such as desorption of pollutants for the regeneration of the active materials, are still a major challenge and need to be thoroughly investigated.

Author details

Rahul Sharma and Parveen Saini*

*Address all correspondence to: pksaini@nplindia.org; parveensaini580@gmail.com

Conjugated Polymer and Graphene Technology Lab, Polymeric and Soft Materials Section, Materials Physics and Engineering Division, CSIR-National Physical Laboratory, New Delhi, India

References

[1] Peter Osei Boama, Jacqueline Onumah, Mohammed Takase, Prince Osei Bonsu & Tayari Salifu. AIR POLLUTION CONTROL TECHNIQUES. *G.J.B.B* 1, 124–131 (2012).

[2] Yang, Y., Gupta, M. C., Dudley, K. L. & Lawrence, R. W. Novel Carbon Nanotube-Polystyrene Foam Composites for Electromagnetic Interference Shielding. *Nano Lett*. 5, 2131–2134 (2005).

[3] Romero, J. V. *et al*. A combinatorial approach to screening carbon based materials for respiratory protection. *J. Hazard. Mater*. 183, 677–687 (2010).

[4] Marchiol, L., Assolari, S., Sacco, P. & Zerbi, G. Phytoextraction of heavy metals by canola (Brassica napus) and radish (Raphanus sativus) grown on multicontaminated soil. *Environ. Pollut*. 132, 21–27 (2004).

[5] Kirkham, M. B. Cadmium in plants on polluted soils: Effects of soil factors, hyperaccumulation, and amendments. *Geoderma* 137, 19–32 (2006).

[6] Khan, F. I. & Kr. Ghoshal, A. Removal of Volatile Organic Compounds from polluted air. *J. Loss Prev. Process Ind*. 13, 527–545 (2000).

[7] Zhang, H., Lv, X., Li, Y., Wang, Y. & Li, J. P25-Graphene Composite as a High Performance Photocatalyst. *Acs Nano* 4, 380–386 (2010).

[8] Zhao, L. *et al*. TiO2–graphene sponge for the removal of tetracycline. *J. Nanoparticle Res*. 17, (2015),17:16

[9] Yang, Y., Yi, H. & Wang, C. Oil Absorbents Based on Melamine/Lignin by a Dip Adsorbing Method. *Acs Sustain. Chem. Eng*. 3, 3012–3018 (2015).

[10] Upadhyay, R. K., Soin, N. & Roy, S. S. Role of graphene/metal oxide composites as photocatalysts, adsorbents and disinfectants in water treatment: a review. *Rsc Adv* 4, 3823–3851 (2014).

[11] Saini,P.(2015) *Fundamentals of Conjugated Polymer Blends, Copolymers and Composites: Synthesis, Properties and Applications*. (John Wiley & Sons, Inc., 2015). Hoboken, NJ, USA. doi: 10.1002/9781119137160.ch1 <http://doi.wiley.com/10.1002/9781119137160>

[12] Saini, P. & Choudhary, V. Enhanced electromagnetic interference shielding effectiveness of polyaniline functionalized carbon nanotubes filled polystyrene composites. *J. Nanoparticle Res*. 15, (2013), 15: 1415

[13] Saini, P. (2013) Electrical Properties and Electromagnetic Interference Shielding Response of Electrically Conducting Thermosetting Nanocomposites, in Thermoset Nanocomposites (ed V. Mittal), Wiley-VCH Verlag GmbH & Co. KGaA, Weinheim, Germany. doi: 10.1002/9783527659647.ch10

[14] Fu, F. & Wang, Q. Removal of heavy metal ions from wastewaters: A review. *J. Environ. Manage*. 92, 407–418 (2011).

[15] Yilmaz, M., Tay, T., Kivanc, M. & Turk, H. Removal of corper(II) Ions from aqueous solution by a lactic acid bacterium. *Braz. J. Chem. Eng*. 27, 309–314 (2010).

[16] Xue, Z., Cao, Y., Liu, N., Feng, L. & Jiang, L. Special wettable materials for oil/water separation. *J Mater Chem* 2, 2445–2460 (2014).

[17] Chandra, V. *et al*. Water-Dispersible Magnetite-Reduced Graphene Oxide Composites for Arsenic Removal. *Acs Nano* 4, 3979–3986 (2010).

[18] Tan, I. A. W., Ahmad, A. L. & Hameed, B. H. Adsorption of basic dye on high-surface-area activated carbon prepared from coconut husk: Equilibrium, kinetic and thermodynamic studies. *J. Hazard. Mater*. 154, 337–346 (2008).

[19] Whitehead, P. G. & Lack, T. Dispersion and self-purification of pollutants in surface water systems. *United Nations Educ. Sci. Cult. Organ. 7 Place Fontenoy 75700 Paris*

[20] El Qada, E. N., Allen, S. J. & Walker, G. M. Adsorption of basic dyes from aqueous solution onto activated carbons. *Chem. Eng. J*. 135, 174–184 (2008).

[21] TOXNET (Toxicology Database Network. at <http://toxnet.nlm.nih.gov/cgi-bin/sis/search/a?dbs+hsdb:@term+@DOCNO+1405>

[22] Sulak, M. T. & Yatmaz, H. C. Removal of textile dyes from aqueous solutions with eco-friendly biosorbent. *Desalination Water Treat*. 37, 169–177 (2012).

[23] Kayode, J., Olowoyo, O. & Oyedeji, A. The Effects of Used Engine Oil Pollution on the Growth and Early Seedling Performance of Vigna uniguiculata and Zea mays. *Res. J. Soil Biol*. 1, 15–19 (2009).

[24] at <https://en.wikipedia.org/wiki/Deepwater_Horizon_oil_spill>

[25] Ordinioha, B. & Brisibe, S. The human health implications of crude oil spills in the Niger delta, Nigeria: An interpretation of published studies. *Niger. Med. J*. 54, 10 (2013).

[26] Dalton, T. & Jin, D. Extent and frequency of vessel oil spills in US marine protected areas. *Mar. Pollut. Bull*. 60, 1939–1945 (2010).

[27] Vazquez-Duhalt, R. Environmental impact of used motor oil. *Sci. Total Environ*. 79, 1–23 (1989).

[28] Bayat, A., Aghamiri, S. F., Moheb, A. & Vakili-Nezhaad, G. R. Oil Spill Cleanup from Sea Water by Sorbent Materials. *Chem. Eng. Technol*. 28, 1525–1528 (2005).

[29] Nwilo, P. C. & Badejo, O. T. OIL SPILL PROBLEMS AND MANAGEMENT IN THE NIGER DELTA. *Int. Oil Spill Conf. Proc*. 2005, 567–570 (2005).

[30] OKOYE & OKUNROBO. IMPACT OF OIL SPILL ON LAND AND WATER AND ITS HEALTH IMPLICATIONS IN ODUGBORO COMMUNITY, SAGAMU, OGUN STATE, NIGERIA. *World J. Environ. Sci. Eng*. 1, 1–21 (2014).

[31] Protecting Our Ocean and Coastal Economies. https://www.nrdc.org/sites/default/files/offshore.pdf dated 24 December, 2015

[32] Joshi, R. K. *et al*. Precise and Ultrafast Molecular Sieving Through Graphene Oxide Membranes. *Science* 343, 752–754 (2014).

[33] Dushenkov, V., Kumar, P. B. A. N., Motto, H. & Raskin, I. Rhizofiltration: The Use of Plants to Remove Heavy Metals from Aqueous Streams. *Environ. Sci. Technol*. 29, 1239–1245 (1995).

[34] Zhang, Y., Tang, Z.-R., Fu, X. & Xu, Y.-J. TiO_2 -Graphene Nanocomposites for Gas-Phase Photocatalytic Degradation of Volatile Aromatic Pollutant: Is TiO_2 -Graphene Truly Different from Other TiO_2 -Carbon Composite Materials? *Acs Nano* 4, 7303–7314 (2010).

[35] Lachheb, H. *et al*. Photocatalytic degradation of various types of dyes (Alizarin S, Crocein Orange G, Methyl Red, Congo Red, Methylene Blue) in water by UV-irradiated titania. *Appl. Catal. B Environ*. 39, 75–90 (2002).

[36] Zhang, X., Liu, D., Yang, L., Zhou, L. & You, T. Self-assembled three-dimensional graphene-based materials for dye adsorption and catalysis. *J Mater Chem* 3, 10031–10037 (2015).

[37] Bi, H. *et al*. Spongy Graphene as a Highly Efficient and Recyclable Sorbent for Oils and Organic Solvents. *Adv. Funct. Mater*. 22, 4421–4425 (2012).

[38] Song, W.-L. *et al*. Tuning three-dimensional textures with graphene aerogels for ultra-light flexible graphene/texture composites of effective electromagnetic shielding. *Carbon* 93, 151–160 (2015).

[39] Wang, C.-F., Huang, H.-C. & Chen, L.-T. Protonated Melamine Sponge for Effective Oil/Water Separation. *Sci. Reports* 5, 14294 (2015).

[40] Broje, V. & Keller, A. A. Improved Mechanical Oil Spill Recovery Using an Optimized Geometry for the Skimmer Surface. *Environ. Sci. Technol*. 40, 7914–7918 (2006).

[41] Goodbody-Gringley, G. *et al*. Toxicity of Deepwater Horizon Source Oil and the Chemical Dispersant, Corexit® 9500, to Coral Larvae. *Plos One* 8, e45574 (2013).

[42] Brooijmans, R. J. W., Pastink, M. I. & Siezen, R. J. Hydrocarbon-degrading bacteria: the oil-spill clean-up crew. *Microb. Biotechnol*. 2, 587–594 (2009).

[43] Zhao, J., Ren, W. & Cheng, H.-M. Graphene sponge for efficient and repeatable adsorption and desorption of water contaminations. *J. Mater. Chem*. 22, 20197 (2012).

[44] Mukherjee, R., Sharma, R., Saini, P. & De, S. Nanostructured polyaniline incorporated ultrafiltration membrane for desalination of brackish water. *Env. Sci Water Res Technol* 1, 893–904 (2015).

[45] Liu, M., Chen, C., Hu, J., Wu, X. & Wang, X. Synthesis of Magnetite/Graphene Oxide Composite and Application for Cobalt(II) Removal. *J. Phys. Chem. C* 115, 25234–25240 (2011).

[46] Zhu, L. *et al*. Mixed matrix membranes containing MIL-53(Al) for potential application in organic solvent nanofiltration. *Rsc Adv* 5, 73068–73076 (2015).

[47] Liu, F., Chung, S., Oh, G. & Seo, T. S. Three-Dimensional Graphene Oxide Nanostructure for Fast and Efficient Water-Soluble Dye Removal. *Acs Appl. Mater. Interfaces* 4, 922–927 (2012).

[48] Li, Q., Zhai, J., Zhang, W., Wang, M. & Zhou, J. Kinetic studies of adsorption of Pb(II), Cr(III) and Cu(II) from aqueous solution by sawdust and modified peanut husk. *J. Hazard. Mater*. 141, 163–167 (2007).

[49] Li, B. & Cao, H. ZnO@graphene composite with enhanced performance for the removal of dye from water. *J Mater Chem* 21, 3346–3349 (2011).

[50] Kornaros, M. & Lyberatos, G. Biological treatment of wastewaters from a dye manufacturing company using a trickling filter. *J. Hazard. Mater*. 136, 95–102 (2006).

[51] Kalantzopoulos, G. N. *et al*. Resistance to the transport of H2 through the external surface of as-made and modified silicalite-1 (MFI). *Microporous Mesoporous Mater*. 220, 290–297 (2016).

[52] Gao, W. *et al*. Engineered Graphite Oxide Materials for Application in Water Purification. *Acs Appl. Mater. Interfaces* 3, 1821–1826 (2011).

[53] Fan, W. *et al*. Hybridization of graphene sheets and carbon-coated Fe3O4 nanoparticles as a synergistic adsorbent of organic dyes. *J. Mater. Chem*. 22, 25108 (2012).

[54] Ackacha, M. A. Removal of Pb(II) from Aqueous Solution by <i>Portulaca oleracea</i> Leaves: Kinetic, Equilibrium and Thermodynamic Studies. *Am. J. Anal. Chem*. 04, 27–32 (2013).

[55] Jiao, T. *et al*. Reduced Graphene Oxide-Based Silver Nanoparticle-Containing Composite Hydrogel as Highly Efficient Dye Catalysts for Wastewater Treatment. *Sci. Reports* 5, 11873 (2015).

[56] Khin, M. M., Nair, A. S., Babu, V. J., Murugan, R. & Ramakrishna, S. A review on nanomaterials for environmental remediation. *Energy Environ. Sci*. 5, 8075 (2012).

[57] Wang, S., Sun, H., Ang, H. M. & Tadé, M. O. Adsorptive remediation of environmental pollutants using novel graphene-based nanomaterials. *Chem. Eng. J*. 226, 336–347 (2013).

[58] Shannon, M. A. *et al*. Science and technology for water purification in the coming decades. *Nature* 452, 301–310 (2008).

[59] Liu, H., Liu, Z., Yang, M. & He, Q. Surperhydrophobic polyurethane foam modified by graphene oxide. *J. Appl. Polym. Sci*. 130, 3530–3536 (2013).

[60] Tran, D. N. H., Kabiri, S., Sim, T. R. & Losic, D. Selective adsorption of oil–water mixtures using polydimethylsiloxane (PDMS)–graphene sponges. *Env. Sci Water Res Technol* 1, 298–305 (2015).

[61] Wang, S. & Peng, Y. Natural zeolites as effective adsorbents in water and wastewater treatment. *Chem. Eng. J*. 156, 11–24 (2010).

[62] Wang, H., Kang, J., Liu, H. & Qu, J. Preparation of organically functionalized silica gel as adsorbent for copper ion adsorption. *J. Environ. Sci*. 21, 1473–1479 (2009).

[63] Kasprzyk-Hordern, B. Chemistry of alumina, reactions in aqueous solution and its application in water treatment. *Adv. Colloid Interface Sci*. 110, 19–48 (2004).

[64] Hui, K., Chao, C. & Kot, S. Removal of mixed heavy metal ions in wastewater by zeolite 4A and residual products from recycled coal fly ash. *J. Hazard. Mater*. 127, 89–101 (2005).

[65] Dias, J. M., Alvim-Ferraz, M. C. M., Almeida, M. F., Rivera-Utrilla, J. & Sánchez-Polo, M. Waste materials for activated carbon preparation and its use in aqueous-phase treatment: A review. *J. Environ. Manage*. 85, 833–846 (2007).

[66] Raposo, F., De La Rubia, M. A. & Borja, R. Methylene blue number as useful indicator to evaluate the adsorptive capacity of granular activated carbon in batch mode: Influence of adsorbate/adsorbent mass ratio and particle size. *J. Hazard. Mater*. 165, 291–299 (2009).

[67] Yan, C., Wang, C., Yao, J., Zhang, L. & Liu, X. Adsorption of methylene blue on mesoporous carbons prepared using acid- and alkaline-treated zeolite X as the template. *Colloids Surfaces Physicochem. Eng. Asp*. 333, 115–119 (2009).

[68] Banat, F., S. Al-Asheh, R. Al-Ahmad & F. Bni-Khalid. Bench-scale and packed bed sorption of methylene blue using treated olive pomace and charcoal,. *Bioresour Technol* 98, 3017–3025 (2007).

[69] Namasivayam, C. & Kavitha, D. Removal of Congo Red from water by adsorption onto activated carbon prepared from coir pith, an agricultural solid waste. *Dyes Pigments* 54, 47–58 (2002).

[70] Ai, L., Li, M. & Li, L. Adsorption of Methylene Blue from Aqueous Solution with Activated Carbon/Cobalt Ferrite/Alginate Composite Beads: Kinetics, Isotherms, and Thermodynamics. *J. Chem. Eng. Data* 56, 3475–3483 (2011).

[71] Foo, K. Y. & Hameed, B. H. Detoxification of pesticide waste via activated carbon adsorption process. *J. Hazard. Mater*. 175, 1–11 (2010).

[72] Sánchez-Polo, M. & Rivera-Utrilla, J. Adsorbent-Adsorbate Interactions in the Adsorption of Cd(II) and Hg(II) on Ozonized Activated Carbons. *Environ. Sci. Technol*. 36, 3850–3854 (2002).

[73] Geim, A.K. & Novoselov, K.S.The rise and rise of graphene. *Nat. Nanotechnol*. 5, 755–755 (2010).

[74] Zhao, G., Li, J., Ren, X., Chen, C. & Wang, X. Few-Layered Graphene Oxide Nanosheets As Superior Sorbents for Heavy Metal Ion Pollution Management. *Environ. Sci. Technol*. 45, 10454–10462 (2011).

[75] Wang, J.-N. *et al*. Recent developments in superhydrophobic graphene and graphene-related materials: from preparation to potential applications. *Nanoscale* 7, 7101–7114 (2015).

[76] Sun, Y., Wu, Q. & Shi, G. Graphene based new energy materials. *Energy Environ. Sci*. 4, 1113 (2011).

[77] Schedin, F. *et al*. Detection of individual gas molecules adsorbed on graphene. *Nat. Mater*. 6, 652–655 (2007).

[78] Li, X. *et al*. Graphene Films with Large Domain Size by a Two-Step Chemical Vapor Deposition Process. *Nano Lett*. 10, 4328–4334 (2010).

[79] Zhu, J. *et al*. One-Pot Synthesis of Magnetic Graphene Nanocomposites Decorated with Core@Double-shell Nanoparticles for Fast Chromium Removal. *Environ. Sci. Technol*. 46, 977–985 (2012).

[80] Xu, J., Wang, L. & Zhu, Y. Decontamination of Bisphenol A from Aqueous Solution by Graphene Adsorption. *Langmuir* 28, 8418–8425 (2012).

[81] Ren, Y. *et al*. Graphene/d-MnO2 composite as adsorbent for the removal of nickel ions from wastewater. *Chem. Eng. J*. 175, 1–7 (2011).

[82] Luo, X. *et al*. Nanocomposites of graphene oxide-hydrated zirconium oxide for simultaneous removal of As(III) and As(V) from water. *Chem. Eng. J*. 220, 98–106 (2013).

[83] Chabot, V. *et al*. A review of graphene and graphene oxide sponge: material synthesis and applications to energy and the environment. *Energy Environ. Sci*. 7, 1564 (2014).

[84] Li, B., Cao, H. & Yin, G. Mg(OH)2@reduced graphene oxide composite for removal of dyes from water. *J. Mater. Chem*. 21, 13765 (2011).

[85] Wang, C.-F. & Lin, S.-J. Robust Superhydrophobic/Superoleophilic Sponge for Effective Continuous Absorption and Expulsion of Oil Pollutants from Water. *Acs Appl. Mater. Interfaces* 5, 8861–8864 (2013).

[86] Nguyen, D. D., Tai, N.-H., Lee, S.-B. & Kuo, W.-S. Superhydrophobic and superoleophilic properties of graphene-based sponges fabricated using a facile dip coating method. *Energy Environ. Sci*. 5, 7908 (2012).

[87] Bosma, W. J. P., Bellin, A., van der Zee, S. E. A. T. M. & Rinaldo, A. Linear equilibrium adsorbing solute transport in physically and chemically heterogeneous porous formations: 2. Numerical results. *Water Resour. Res*. 29, 4031–4043 (1993).

[88] Dutta, S. K. & Singh, D. Sorption and desorption behavior of lead in four different soils of India. *Agric. Sci*. 02, 41–48 (2011).

[89] Carrasco-Marin, F., Lopez-Ramon, M. V. & Moreno-Castilla, C. Applicability of the Dubinin-Radushkevich equation to carbon dioxide adsorption on activated carbons. *Langmuir* 9, 2758–2760 (1993).

[90] Peric, J., Trgo, M. & Vukojevic Medvidovic, N. Removal of zinc, copper and lead by natural zeolite—a comparison of adsorption isotherms. *Water Res*. 38, 1893–1899 (2004).

[91] Moreno-Castilla, C., Álvarez-Merino, M. A., López-Ramón, M. V. & Rivera-Utrilla, J. Cadmium Ion Adsorption on Different Carbon Adsorbents from Aqueous Solutions. Effect of Surface Chemistry, Pore Texture, Ionic Strength, and Dissolved Natural Organic Matter. *Langmuir* 20, 8142–8148 (2004).

[92] S, L. About the theory of so-called adsorption of soluble substances. *K Sven Vetenskapsakad Handl* 24, 1–39 (1898).

[93] Kooli, F., Yan, L., Al-Faze, R. & Al-Sehimi, A. Removal enhancement of basic blue 41 by brick waste from an aqueous solution. *Arab. J. Chem*. 8, 333–342 (2015).

[94] Mahmoodi, N. M. Equilibrium, Kinetics, and Thermodynamics of Dye Removal Using Alginate in Binary Systems. *J. Chem. Eng. Data* 56, 2802–2811 (2011).

[95] Ho, Y. . & McKay, G. Pseudo-second order model for sorption processes. *Process Biochem*. 34, 451–465 (1999).

[96] Karagoz, S., Tay, T., Ucar, S. & Erdem, M. Activated carbons from waste biomass by sulfuric acid activation and their use on methylene blue adsorption. *Bioresour. Technol*. 99, 6214–6222 (2008).

[97] Wu, X.-L., Wang, L., Chen, C.-L., Xu, A.-W. & Wang, X.-K. Water-dispersible magnetite-graphene-LDH composites for efficient arsenate removal. *J. Mater. Chem*. 21, 17353 (2011).

[98] Wang, M., Lawal, A., Stephenson, P., Sidders, J. & Ramshaw, C. Post-combustion CO2 capture with chemical absorption: A state-of-the-art review. *Chem. Eng. Res. Des*. 89, 1609–1624 (2011).

[99] Vácha, R., Slavíc?ek, P., Mucha, M., Finlayson-Pitts, B. J. & Jungwirth, P. Adsorption of Atmospherically Relevant Gases at the Air/Water Interface: Free Energy Profiles of Aqueous Solvation of N_2, O_2, O_3, OH, H_2O, HO_2, and H_2O_2. *J. Phys. Chem. A* 108, 11573–11579 (2004).

[100] Wang, S., Li, M. & Lu, Q. Filter Paper with Selective Absorption and Separation of Liquids that Differ in Surface Tension. *Acs Appl. Mater. Interfaces* 2, 677–683 (2010).

[101] Baldacchini, T., Carey, J. E., Zhou, M. & Mazur, E. Superhydrophobic Surfaces Prepared by Microstructuring of Silicon Using a Femtosecond Laser. *Langmuir* 22, 4917–4919 (2006).

[102] Wenzel, R. N. RESISTANCE OF SOLID SURFACES TO WETTING BY WATER. *Ind. Eng. Chem*. 28, 988–994 (1936).

[103] Cassie, A. B. D. & Baxter, S. Wettability of porous surfaces. *Trans. Faraday Soc*. 40, 546 (1944).

[104] Rizzuti, L. & Brucato, A. Liquid viscosity and flow rate effects on interfacial area in packed columns. *Chem. Eng. J*. 41, 49–52 (1989).

[105] Liu, Y. *et al*. Cost-Effective Reduced Graphene Oxide-Coated Polyurethane Sponge As a Highly Efficient and Reusable Oil-Absorbent. *Acs Appl. Mater. Interfaces* 5, 10018–10026 (2013).

[106] Gupta, S. S., Sreeprasad, T. S., Maliyekkal, S. M., Das, S. K. & Pradeep, T. Graphene from Sugar and its Application in Water Purification. *Acs Appl. Mater. Interfaces* 4, 4156–4163 (2012).

[107] Chen, Y., Chen, L., Bai, H. & Li, L. Graphene oxide–chitosan composite hydrogels as broad-spectrum adsorbents for water purification. *J Mater Chem* 1, 1992–2001 (2013).

[108] Wang, C. *et al*. Preparation of a graphene-based magnetic nanocomposite for the removal of an organic dye from aqueous solution. *Chem. Eng. J*. 173, 92–97 (2011).

[109] Lü, W., Wu, Y., Chen, J. & Yang, Y. Facile preparation of graphene–Fe_3O_4 nanocomposites for extraction of dye from aqueous solution. *CrystEngComm* 16, 609–615 (2014).

[110] Jiang, Y. *et al*. Magnetic chitosan–graphene oxide composite for anti-microbial and dye removal applications. *Int. J. Biol. Macromol*. 82, 702–710 (2016).

[111] Samad, Y. A., Li, Y., Schiffer, A., Alhassan, S. M. & Liao, K. Graphene Foam Developed with a Novel Two-Step Technique for Low and High Strains and Pressure-Sensing Applications. *Small* 11, 2380–2385 (2015).

[112] Sharma, P., Hussain, N., Borah, D. J. & Das, M. R. Kinetics and Adsorption Behavior of the Methyl Blue at the Graphene Oxide/Reduced Graphene Oxide Nanosheet–Water Interface: A Comparative Study. *J. Chem. Eng. Data* 58, 3477–3488 (2013).

[113] Fan, L., Luo, C., Sun, M. & Qiu, H. Synthesis of graphene oxide decorated with magnetic cyclodextrin for fast chromium removal. *J. Mater. Chem*. 22, 24577 (2012).

[114] Hao, L. *et al*. SiO2/graphene composite for highly selective adsorption of Pb(II) ion. *J. Colloid Interface Sci*. 369, 381–387 (2012).

[115] Alyüz, B. & Veli, S. Kinetics and equilibrium studies for the removal of nickel and zinc from aqueous solutions by ion exchange resins. *J. Hazard. Mater*. 167, 482–488 (2009).

[116] Rafatullah, M., Sulaiman, O., Hashim, R. & Ahmad, A. Adsorption of methylene blue on low-cost adsorbents: A review. *J. Hazard. Mater*. 177, 70–80 (2010).

[117] Li, B., Cao, H., Yin, J., Wu, Y. A. & Warner, J. H. Synthesis and separation of dyesvia Ni@reduced graphene oxide nanostructures. *J Mater Chem* 22, 1876–1883 (2012).

[118] Sun, H., Xu, Z. & Gao, C. Multifunctional, Ultra-Flyweight, Synergistically Assembled Carbon Aerogels. *Adv. Mater*. 25, 2554–2560 (2013).

[119] Tjandra, R. *et al*. Introduction of an Enhanced Binding of Reduced Graphene Oxide to Polyurethane Sponge for Oil Absorption. *Ind. Eng. Chem. Res*. 54, 3657–3663 (2015).

IntechOpen